Molecular Cell

Article

Formation of toxic oligomers of polyQ-expanded Huntingtin by prion-mediated cross-seeding

Graphical abstract

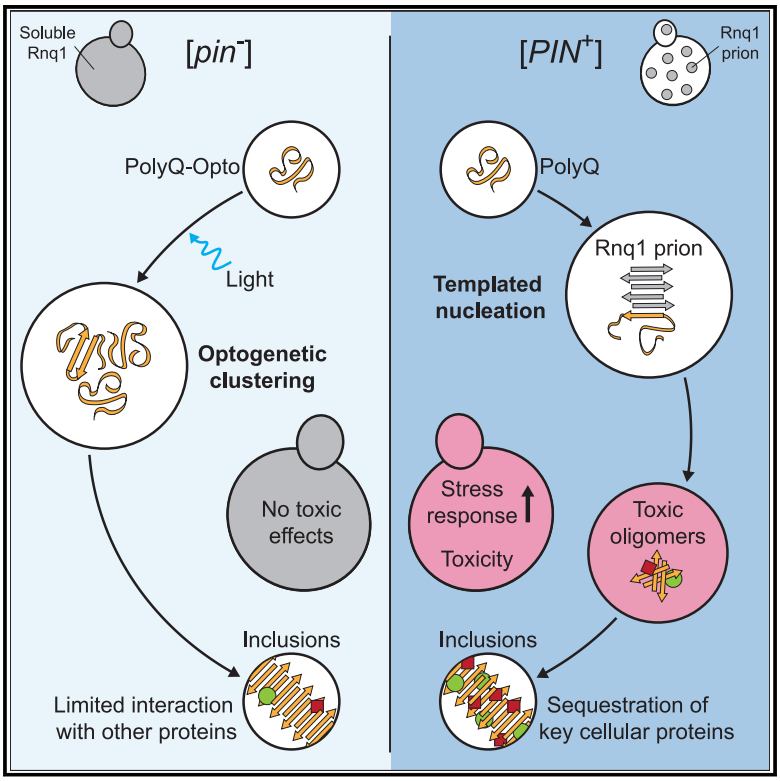

Highlights

- Optogenetic clustering allows prion-independent polyQ protein aggregation in yeast
- Light-induced aggregation circumvents formation of toxic polyQ oligomers
- Toxic polyQ oligomers form dependent on templating by Rnq1 prions
- Age-dependent prion-like aggregates may induce toxic polyQ oligomers in disease

Authors

Michael H.M. Gropp, Courtney L. Klaips, F. Ulrich Hartl

Correspondence

c.l.klaips@umcg.nl (C.L.K.), uhartl@biochem.mpg.de (F.U.H.)

In brief

Protein aggregation is a hallmark of many neurodegenerative diseases. Using an optogenetic approach in *Saccharomyces cerevisiae*, Gropp et al. demonstrate that toxic oligomers of a disease protein are generated through cross-seeding by pre-existing cellular prions. The authors speculate that similar mechanisms may be involved in toxic aggregate formation in disease.

Gropp et al., 2022, Molecular Cell *82*, 4290–4306
November 17, 2022
https://doi.org/10.1016/j.molcel.2022.09.031

CellPress

CellPress

Molecular Cell

Article

Formation of toxic oligomers of polyQ-expanded Huntingtin by prion-mediated cross-seeding

Michael H.M. Gropp,[1] Courtney L. Klaips,[1,3,*] and F. Ulrich Hartl[1,2,4,*]

[1]Department of Cellular Biochemistry, Max Planck Institute of Biochemistry, Am Klopferspitz 18, 82152 Martinsried, Germany

[2]Munich Cluster for Systems Neurology (SyNergy), Munich, Germany

[3]Department of Biomedical Sciences of Cells & Systems, University Medical Center Groningen, Antonius Deusinglaan 1, 9713AV Groningen, the Netherlands

[4]Lead contact

*Correspondence: c.l.klaips@umcg.nl (C.L.K.), uhartl@biochem.mpg.de (F.U.H.)

https://doi.org/10.1016/j.molcel.2022.09.031

SUMMARY

Manifestation of aggregate pathology in Huntington's disease is thought to be facilitated by a preferential vulnerability of affected brain cells to age-dependent proteostatic decline. To understand how specific cellular backgrounds may facilitate pathologic aggregation, we utilized the yeast model in which polyQ-expanded Huntingtin forms aggregates only when the endogenous prion-forming protein Rnq1 is in its amyloid-like prion [*PIN*$^+$] conformation. We employed optogenetic clustering of polyQ protein as an orthogonal method to induce polyQ aggregation in prion-free [*pin*$^-$] cells. Optogenetic aggregation circumvented the prion requirement for the formation of detergent-resistant polyQ inclusions but bypassed the formation of toxic polyQ oligomers, which accumulated specifically in [*PIN*$^+$] cells. Reconstitution of aggregation *in vitro* suggested that these polyQ oligomers formed through direct templating on Rnq1 prions. These findings shed light on the mechanism of prion-mediated formation of oligomers, which may play a role in triggering polyQ pathology in the patient brain.

INTRODUCTION

Toxic protein aggregation is a hallmark of a group of age-dependent neurodegenerative conditions, including Alzheimer's, Parkinson's, and Huntington's diseases. Understanding the basic cytopathology in these disorders, especially with regard to the biochemical principles of protein aggregation, holds promise for the development of urgently needed therapeutics (Chiti and Dobson, 2017; Gandhi et al., 2019; Hartl, 2017; Ross and Poirier, 2004; Stefani and Dobson, 2003). In Huntington's disease (HD) aggregation is mediated by a dominantly inherited polyglutamine (polyQ) expansion in the respective disease protein (Walker, 2007). The pathological polyQ expansion in Huntingtin varies in length from 36 to >100 Q, with longer repeats resulting in higher aggregation propensity and earlier age of disease onset (Gusella and MacDonald, 2000; Kremer et al., 1994). Similar to other neurodegenerative disease proteins, Huntingtin is ubiquitously expressed within the central nervous system and beyond, but aggregate pathology and neuronal dysfunction typically initiates in the striatal neurons of the subcortical basal ganglia (Fu et al., 2018; Walker, 2007). This effect of the cellular background in facilitating toxic aggregation has been attributed in part to a preferential vulnerability of the affected cells to a generalized proteostatic decline during aging (Balch et al., 2008; Douglas and Dillin, 2010; Hipp et al., 2014; Klaips et al., 2018; Labbadia and Morimoto, 2015). Aggregation of specific disease proteins may directly result from reduced availability of molecular chaperones in proteostasis-compromised cells. Alternatively, pathologic aggregates may be triggered by other protein aggregates through cross-seeding (Giasson et al., 2003; Guo et al., 2013; Morales et al., 2013; Vasconcelos et al., 2016). These mechanisms are not mutually exclusive, as reduced proteostasis capacity could increase levels of seeding-competent protein aggregates and vice versa. Disentangling the individual contributions of these two potential aggregation triggers remains a substantial hurdle in studying the biology of protein aggregation.

The yeast *S. cerevisiae* is a powerful model system to explore fundamental principles underlying the aggregation of neurodegenerative disease proteins and the cellular responses to the aggregation process (De Vos et al., 2011; Di Gregorio and Duennwald, 2018; Duennwald, 2011; Moosavi et al., 2015; Verghese et al., 2012; Winderickx et al., 2008), including polyQ-length-dependent Huntingtin aggregation and its modulation by chaperones (Krobitsch and Lindquist, 2000; Muchowski et al., 2000). As with other disease proteins, current models suggest that the major toxic polyQ species are soluble oligomers

(Arrasate et al., 2004; Behrends et al., 2006; Kayed et al., 2003; Leitman et al., 2013; Schaffar et al., 2004; Takahashi et al., 2008) that accumulate in a process of nucleated conformational conversion, both in mammalian cells and in the yeast model (Ossato et al., 2010; Sinnige et al., 2021; Walters and Murphy, 2011; Wetzel, 2012). Toxic oligomers may interfere with cellular membrane integrity and/or engage in aberrant interactions with endogenous proteins, including proteostasis components, possibly resulting in the sequestration of essential factors within insoluble inclusions (Bäuerlein et al., 2017; Kim et al., 2002, 2016; Olzscha et al., 2011; Park et al., 2013).

The cellular environment can profoundly modulate the aggregation of disease-relevant proteins. A striking example is the dependence of polyQ aggregation and toxicity on the prion strain background in yeast, where polyQ expansion proteins form detergent-resistant inclusions only when the prion-forming protein Rnq1 is present in its amyloid-like prion conformation, [*PIN*$^+$] (Duennwald et al., 2006a; Meriin et al., 2002; Osherovich and Weissman, 2001). Rnq1, a 43 kDa protein of unknown function, contains a prion domain with glutamine- and asparagine-rich low complexity regions (LCRs) that mediates aggregate formation and propagation to daughter cells (Sondheimer and Lindquist, 2000; Vitrenko et al., 2007; Wickner, 2016). Numerous prion-like proteins with similar LCRs have been identified in mammalian cells and tissues, including specific brain regions (Iglesias et al., 2019; March et al., 2016), and have been observed to undergo age-dependent aggregation (Harel et al., 2022; Vecchi et al., 2020; Walther et al., 2015). A mechanistic explanation for the prion dependence of polyQ aggregation in yeast is still missing (Liebman and Chernoff, 2012; Osherovich and Weissman, 2002; Serio, 2018) and the role of prion-like proteins in forming disease-relevant amyloids have remained unclear. It has been suggested that the presence of pre-existing prions can lead to cross-templating of other aggregation-prone proteins, including other yeast prions such as [*PSI*$^+$] (Bradley et al., 2002; Derkatch et al., 1997, 2001, 2004; Gokhale et al., 2005; Meriin et al., 2002; Osherovich and Weissman, 2001; Vitrenko et al., 2007; Wickner et al., 2001). Alternatively, prions may sequester critical proteostasis factors or interfere with stress response pathways, thereby indirectly facilitating protein misfolding and aggregation (Douglas et al., 2008; Lopez et al., 2003; Osherovich and Weissman, 2001; Sondheimer et al., 2001; Wickner et al., 2001).

To obtain insight into the mechanism of prion-mediated polyQ aggregation, we sought to bypass the prion requirement using an optogenetic approach to induce local clustering of polyQ protein. To this end, we employed the *Arabidopsis thaliana* photoreceptor protein cryptochrome 2 (CRY2) as an optogenetic tool. CRY2 forms transient homo-oligomeric protein clusters in response to a blue light stimulus (Más et al., 2000). Upon illumination, the FAD chromophore of CRY2 is reduced by electron transfer from a conserved triad of tryptophan residues leading to conformational changes (Ma et al., 2020; Palayam et al., 2021) that result in reversible homo-oligomer formation. CRY2-mediated protein oligomerization has been applied in plants, human cell culture and various model organisms (Bugaj et al., 2013; Kyung et al., 2015; Pathak et al., 2017; Wang and Lin, 2020) and has been used in light-controlled biocondensate formation (Shin et al., 2017). By fusing CRY2 with the polyQ-expanded Huntingtin exon 1 fragment, we generated SDS-resistant polyQ aggregates in [*pin*$^-$] yeast in a manner dependent on the length of the polyQ tract. The ability to compare polyQ aggregation in isogenic [*PIN*$^+$] and [*pin*$^-$] strains allowed us to study the influence of the cellular background on the aggregation process and the resulting cellular responses. We ruled out differences in global proteome composition or proteostasis capacity between [*PIN*$^+$] and [*pin*$^-$] strains. Surprisingly, the optogenetic induction of polyQ inclusions in [*pin*$^-$] cells failed to cause toxic effects, which could be attributed to the absence of soluble polyQ oligomers. Biologically active polyQ oligomers only formed in [*PIN*$^+$] cells, apparently through direct templating of soluble polyQ species by Rnq1 prions, as demonstrated by *in vitro* reconstitution experiments. These findings provide mechanistic insight into the role of prions in the formation of polyQ oligomers, raising the intriguing possibility that similar mechanisms may contribute to triggering polyQ pathology in the patient brain.

RESULTS

Prion status is not associated with a general proteostasis defect

To confirm the dependence of polyQ protein aggregation on the prion status of yeast cells, we expressed 97Q-mCherry (97Q), a model protein based on Huntingtin (Htt) exon 1 containing a 97Q glutamine (Q) expansion. 20Q-mCherry (20Q) served as control protein with a polyQ length below the aggregation threshold (Krobitsch and Lindquist, 2000; Muchowski et al., 2000). [*PIN*$^+$] cells developed cytosolic inclusions of 97Q, while 20Q remained diffusely distributed (Duennwald et al., 2006a; Meriin et al., 2002; Osherovich and Weissman, 2001) (Figure S1A). To cure the prion phenotype, we treated [*PIN*$^+$] cells with 3 mM guanidine hydrochloride (GdnHCl) to transiently inhibit the AAA+ chaperone Hsp104, which is required for prion maintenance and propagation (Cox et al., 2007; Derkatch et al., 1997; Tuite et al., 1981) (Figure S1B). The resultant [*pin*$^-$] cells no longer formed polyQ inclusions (Meriin et al., 2002) (Figure S1A).

To determine whether the prion state is associated with a general impairment of proteostasis capacity, we first analyzed the total proteome of [*PIN*$^+$] and [*pin*$^-$] cells (Figure 1A). Based on the quantification of ~3,500 proteins, we observed only minor differences between the isogenic strains, with the few proteins significantly enriched ($\geq$ 1.5-fold; $p < 0.05$) in either condition showing no link with proteostasis-relevant processes (Figure 1B; Table S2). To identify factors that may be functionally depleted by sequestration in prion aggregates, we expressed *RNQ1-GFP* in [*PIN*$^+$] cells and immunoprecipitated Rnq1-GFP aggregates from cell lysates, followed by mass spectrometry. Soluble Rnq1-GFP in [*pin*$^-$] cells served as control. Aggregated Rnq1-GFP interacted with numerous proteins with prion-like domains rich in glutamine and asparagine (Figure 1C; Table S3). Such proteins possess LCRs with a high degree of structural flexibility and tend to be sequestered by amyloid aggregates (Hosp et al., 2017; Kim et al., 2016; Olzscha et al., 2011; Park et al., 2013). Additionally, aggregated Rnq1-GFP bound several components of the Hsp70 chaperone system (Ssa1, Ssa2, and Ssa4), with the essential Hsp40 cochaperone Sis1 being most enriched

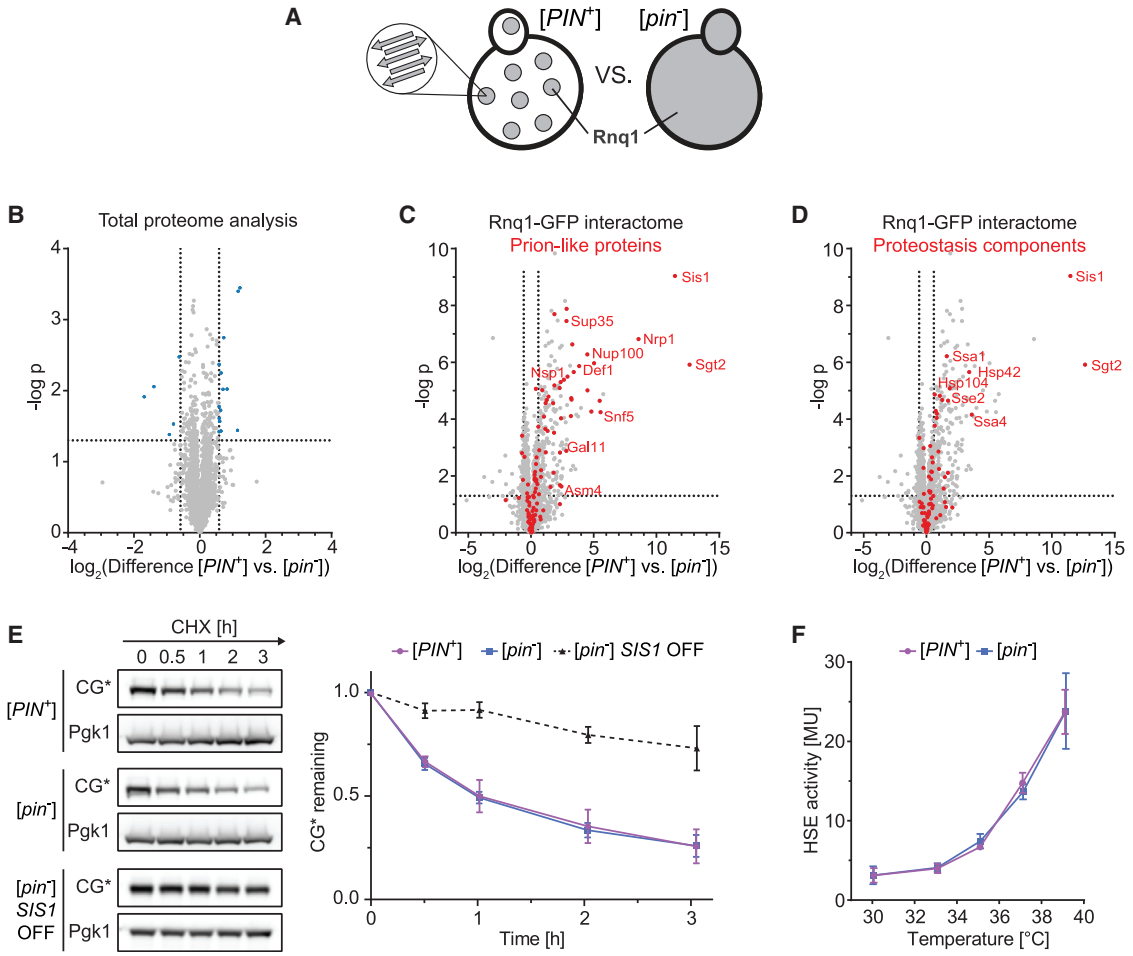

Figure 1. Rnq1 prion status does not detectably impair proteostasis

(A) Schematic of mass spectrometry experiments to compare total proteome composition and the Rnq1 interactome in [*PIN*$^+$] and [*pin*$^-$] yeast strains.

(B) Volcano plot representation of label-free total proteome analysis of [*PIN*$^+$] versus [*pin*$^-$] cells (n = 4). Significantly enriched proteins (≥1.5-fold, $p < 0.05$) are marked in blue.

(C and D) Volcano plot representations of label-free interactome analysis of Rnq1-GFP in [*PIN*$^+$] versus [*pin*$^-$] after anti-GFP immunoprecipitation (IP) (n = 4). Prion-like proteins (C) or chaperones, heat shock proteins and proteins with described protein folding function (D) are labeled in red. Selected proteins are annotated.

(E) Turnover of CG* in [*PIN*$^+$] and [*pin*$^-$] yeast. CG* was expressed in [*PIN*$^+$] and [*pin*$^-$] yeast cells, or a control strain containing a *tet*-repressible *SIS1*, for 20 h. Cycloheximide (CHX) was added to inhibit protein synthesis and cells were collected at the indicated times. Samples were analyzed by SDS-PAGE and immunoblotting for GFP and Pgk1, followed by densitometric analysis. Data represent mean ± SD (n = 3).

(F) Inducibility of the cytosolic heat stress response. β-Galactosidase activity was measured in [*PIN*$^+$] or [*pin*$^-$] cells expressing a LacZ reporter under the control of a minimal promoter containing a heat shock element (HSE) from *SSA3* (pHSELacZ). Cells were grown at 30°C for ~20 h, followed by a shift to the indicated temperature for 1 h. Data represent mean ± SD (n = 4).

See also Figure S1 and Tables S2 and S3.

(Douglas et al., 2008; Lopez et al., 2003; Sondheimer et al., 2001) (Figure 1D; Table S3).

To test whether the sequestration of chaperones in [*PIN*$^+$] cells was sufficient to measurably reduce proteostasis, we analyzed the turnover of cytosolic carboxypeptidase Y* fused to GFP (CG*), a terminally misfolded model protein. CG* undergoes rapid proteasomal degradation upon synthesis in a manner dependent on Hsp70 and Hsp40 (Sis1) (Park et al., 2013). Consequently, Sis1 depletion led to marked stabilization and accumulation of CG* (Park et al., 2013) (Figures 1E and S1C). However, there was no observable difference in CG* turnover between [*PIN*$^+$] and [*pin*$^-$] cells (Figure 1E). Furthermore, activation of the cytosolic heat stress response (HSR), a heat shock transcription factor 1 (Hsf1)-mediated mechanism cells use to sense conditions of conformational stress, can serve as a readout for the state of proteostasis (Anckar and Sistonen, 2011). The HSR was not activated in [*PIN*$^+$] cells and remained inducible by elevated temperature as in [*pin*$^-$] cells, as demonstrated using a β-galactosidase reporter under Hsf1 control (Figure 1F).

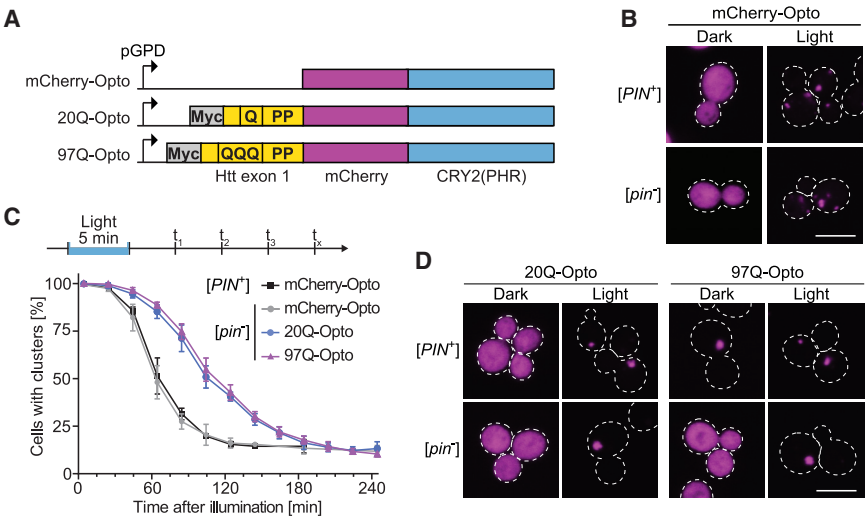

Figure 2. Light-inducible polyQ aggregation

(A) mCherry-Opto consists of the photolyase homology region from CRY2 (PHR) and N-terminal mCherry fluorescent protein. Functionalized Opto constructs additionally contain cMyc-tagged Htt exon 1 with variable polyQ expansion (QQQ) at the N terminus (20Q-Opto and 97Q-Opto). Opto constructs were integrated into the genome and expressed constitutively under the control of the *GPD* promoter.

(B) Light-induced aggregation of mCherry-Opto in [*PIN*$^+$] and [*pin*$^-$] yeast. Cells expressing mCherry-Opto were grown in the absence (dark) or presence (light) of blue light for 6 h. Experiments were performed in triplicate; representative confocal micrographs are shown. Scale bars, 5 μm.

(C) Reversibility of light-induced clustering after short illumination. Quantification of the number of [*PIN*$^+$] or [*pin*$^-$] cells expressing mCherry-, 20Q- or 97Q-Opto in visible clusters at the indicated times after illumination with blue light for 5 min. Each data point represents the mean ± SD from 3 biological replicates (100 cells analyzed per replicate).

(D) Light-induced aggregation of 20Q-Opto and 97Q-Opto in [*PIN*$^+$] and [*pin*$^-$] yeast. Cells expressing the indicated construct were grown in the absence (dark) or presence (light) of blue light for 6 h. Experiments were performed in triplicate; representative confocal micrographs are shown. Scale bars, 5 μm. See also Figure S2.

In summary, while the prion aggregates in [*PIN*$^+$] cells interact with numerous factors, this does not result in an overt proteostasis defect under laboratory growth conditions.

Optogenetic formation of polyQ aggregates in [*pin*$^-$] cells

PolyQ aggregate nucleation is a stochastic process that may be facilitated by initial phase separation of polyQ expansion proteins into a liquid-like condensate (Peskett et al., 2018; Sinnige et al., 2021). We reasoned that the "catalytic" function of the prion phenotype in aggregate formation might be circumvented by artificially clustering the polyQ protein using the photolyase homology region (PHR) of the *A. thaliana* CRY2 protein (Figure 2A), which rapidly forms oligomers upon blue light illumination. To this end, we fused 20Q and 97Q with the CRY2 PHR (20Q-Opto and 97Q-Opto) (Figure 2A).

To demonstrate the light-dependent clustering of CRY2 in yeast cells, we expressed a fusion protein of CRY2 PHR with mCherry (mCherry-Opto) under the control of the constitutive *GPD* promoter (Figure 2A). Note that we used the E490G mutant of CRY2 PHR, known as CRY2Olig, which shows enhanced clustering (Duan et al., 2017; Taslimi et al., 2014). mCherry-Opto was diffusely distributed in the dark but formed distinct foci upon illumination with blue light in both [*PIN*$^+$] and [*pin*$^-$] cells (Figure 2B). Following a short light exposure (5 min), the clusters resolved over time in the dark ($t_{1/2}$ ~60 min) (Figure 2C). mCherry-Opto condensates were detected in a filter retardation assay, but readily dissociated in the presence of SDS (Figure S2A). Furthermore, light-induced clustering neither induced the HSR nor did it interfere with HSR induction by heat stress (Figure S2B), suggesting that the mCherry-Opto condensate is largely inert.

20Q-Opto, was diffusely distributed in the absence of light in both [*PIN*$^+$] and [*pin*$^-$] cells but clustered upon illumination (Figure 2D) like mCherry-Opto (Figure 2B). The polyQ-expanded 97Q-Opto behaved differently, dependent on prion status (Figure 2D). In [*PIN*$^+$] cells, inclusions formed in the dark in a subset of cells. Upon illumination, these preformed inclusions were not altered, while residual diffusely distributed 97Q-Opto clustered into foci (Figure 2D). In the non-permissive [*pin*$^-$] background, 97Q-Opto formed visible foci only in the presence of light (Figure 2D). However, illumination for 5 min did not result in nucleation of stable polyQ-Opto aggregates, although the light-induced clusters dissociated with slower kinetics ($t_{1/2}$ ~110 min) compared with mCherry-Opto (Figure 2C), suggesting transient interactions between polyQ sequences.

We reasoned that nucleation of stable polyQ-Opto aggregates in [*pin*$^-$] cells might require prolonged light-dependent clustering by continuous illumination during cell growth (Figure S3A). PolyQ aggregates in [*PIN*$^+$] yeast and in mammalian cells are partially SDS-resistant, a characteristic feature that mimics the behavior of polyQ fibrils (Kazantsev et al., 1999; Muchowski et al., 2002; Scherzinger et al., 1997). 97Q-Opto in [*PIN*$^+$] cells formed SDS-resistant aggregates without light activation, as detected by filter assay, and continuous illumination strongly enhanced this effect (Figure 3A). Strikingly, prolonged light exposure of [*pin*$^-$] cells also induced SDS-resistant aggregates of 97Q-Opto, but not 20Q-Opto (Figure 3A). In contrast, reversible clustering by illumination for only 5 min failed to nucleate SDS-resistant 97Q-Opto aggregates (Figure S3B). Of note, expression and light activation of the Opto constructs did not alter the [*pin*$^-$] status of the yeast strain (Figure S3C).

To compare the physico-chemical properties of the SDS-resistant aggregates formed via light-induced clustering in [*pin*$^-$] cells with those formed in the [*PIN*$^+$] background, we analyzed aggregate stability upon treatment with detergent or formic acid (Figure 3B). Formic acid has been shown to dissociate polyQ fibrils (Hazeki et al., 2000). The aggregates from both strain backgrounds showed a similar susceptibility to

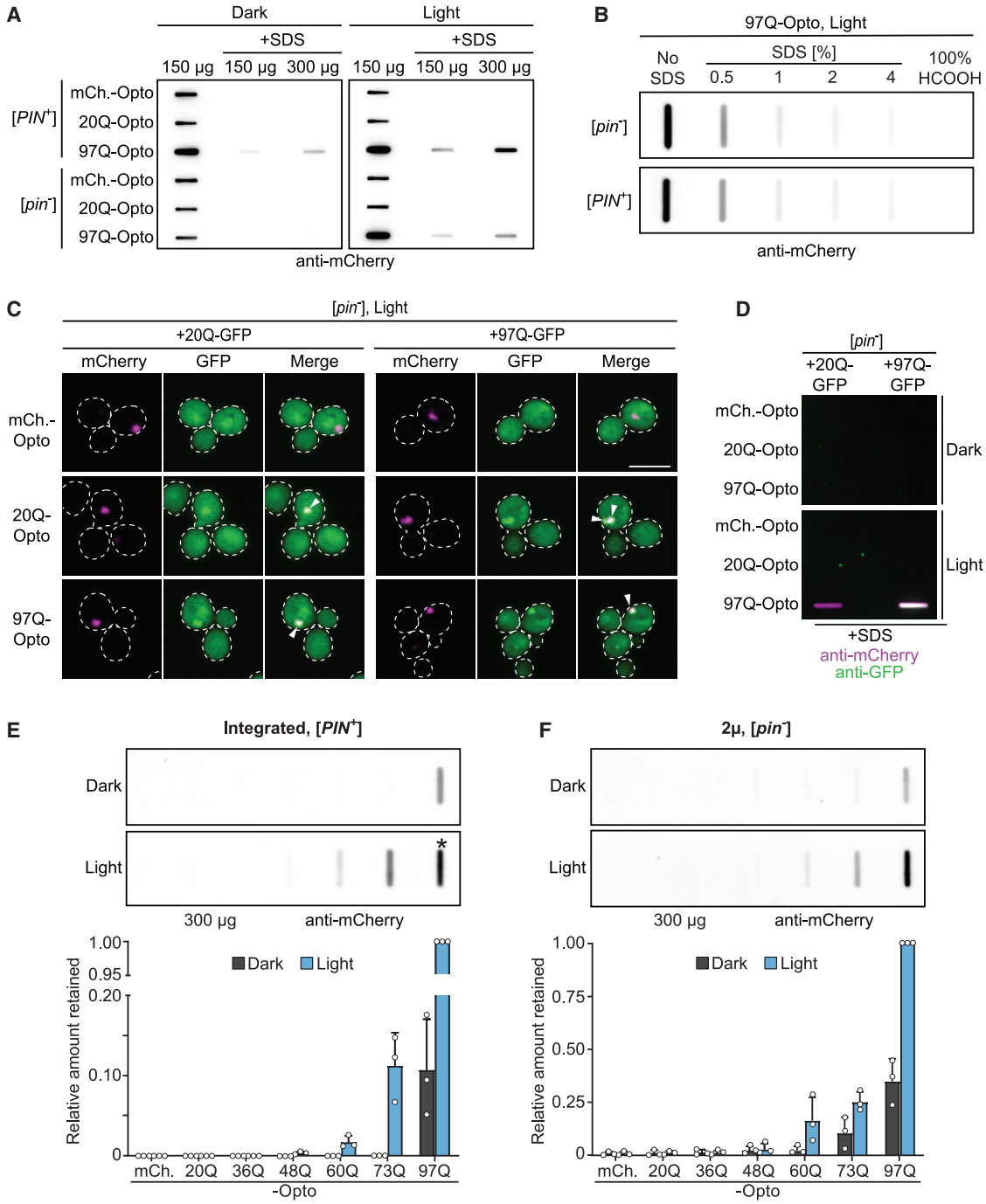

Figure 3. Light-induced formation of polyQ aggregates in [*pin*⁻] cells

(A) The Opto proteins indicated were expressed in [*PIN*⁺] or [*pin*⁻] cells in the absence (dark) or presence (light) of blue light for 20 h. Cell lysates were analyzed by filter assay. Amounts of total protein analyzed are indicated. Opto proteins were detected with anti-mCherry antibody. A representative result is shown from experiments performed in triplicate.

(B) 97Q-Opto was expressed in [*PIN*⁺] or [*pin*⁻] cells from a 2µ plasmid under a galactose-inducible promoter in inducing media for ~23 h in the presence of blue light. Cell lysates were subjected to treatment with different amounts of SDS or 100% formic acid, followed by filter assay as in (A). 375 µg total protein were loaded for each [*pin*⁻] sample, 300 µg for [*PIN*⁺] samples. Only half the amount of total protein was applied in control samples (no SDS). A representative result is shown from experiments performed in triplicate.

(C) Co-aggregation of 20Q-GFP and 97Q-GFP with light-induced polyQ-Opto aggregates. [*pin*⁻] cells coexpressing the proteins indicated were grown in blue light for 20 h. Experiments were performed in triplicate; representative confocal micrographs are shown. Arrows mark colocalization of polyQ proteins. Scale bars, 5 µm.

(legend continued on next page)

increasing concentrations of SDS and dissolved readily in formic acid (Figure 3B), suggesting that they share characteristic structural properties.

Aggregates of polyQ expansion proteins in [*PIN*$^+$] yeast have the ability to sequester proteins with short polyQ sequences that otherwise do not aggregate on their own (Chen et al., 2001; Duennwald et al., 2006a; Kazantsev et al., 1999; Wang et al., 2009). We next tested this property for the polyQ-Opto proteins in [*pin*$^-$] cells coexpressing 20Q-GFP or 97Q-GFP. As expected, the light-induced condensates of mCherry-Opto failed to sequester either 20Q- or 97Q-GFP (Figure 3C). However, both 20Q-GFP and 97Q-GFP co-localized with the light-induced aggregates of 20Q- and 97Q-Opto (Figure 3C). The ability of 20Q-Opto aggregates to sequester polyQ proteins is surprising, as this property had so far only been observed for proteins with expanded polyQ tracts (Duennwald et al., 2006a; Wang et al., 2009). Apparently, co-aggregation of polyQ proteins depends on a locally high polyQ concentration, achieved by light-induced clustering, and does not require a pathological polyQ length. Moreover, polyQ protein co-aggregation is independent of SDS-resistance, as the light-induced 20Q-Opto aggregates remain SDS soluble (Figure 3A). Formation of SDS-resistant co-aggregates was only observed when coexpressing the polyQ-expanded constructs 97Q-Opto and 97Q-GFP (Figure 3D).

The Opto constructs offered the possibility to explore the effects of polyQ length as well as local and overall polyQ concentration on aggregation. We first achieved a low concentration of polyQ constructs by integrating their expression cassette into the genome. Under this regime, only [*PIN*$^+$] cells expressing the longest polyQ track tested (97Q-Opto) accumulated SDS-resistant aggregates in the absence of light (Figure 3E). Light-induced clustering increased the amount of SDS-resistant 97Q-Opto aggregates by more than 10-fold and reduced the threshold length of aggregation to 48 Q (Figure 3E). At higher concentrations, achieved by overexpressing the polyQ constructs from a multicopy 2μ plasmid, a repeat length of 60 Q was sufficient for SDS-resistant aggregation in the dark, with light-induced clustering enhancing aggregation further (Figure S3D). In the non-permissive [*pin*$^-$] background, only 97Q-Opto formed SDS-resistant aggregates upon light induction at the low expression level (Figure S3E). Aggregation remained ~4-fold lower than in illuminated [*PIN*$^+$] cells (Figure 3A), indicating that the [*PIN*$^+$] prion status strongly increases polyQ aggregation propensity. However, upon 2μ overexpression of polyQ-Opto in [*pin*$^-$] cells, light-dependent aggregation clearly shifted to shorter polyQ lengths (Figure 3F), similar to the observations in [*PIN*$^+$] cells (Figure S3D). Notably, at these high polyQ levels, small but detectable amounts of SDS-resistant 97Q-Opto formed even without illumination (Figure 3F).

Taken together, the light-induced polyQ aggregates in [*pin*$^-$] cells share key properties with polyQ inclusions of [*PIN*$^+$] yeast: they are partially SDS-resistant, sequester otherwise soluble polyQ proteins, and are similarly dependent on both polyQ length and protein concentration for formation.

Toxic polyQ oligomers form specifically in [*PIN*$^+$] cells

The possibility to induce and modulate polyQ aggregation with light allowed us to compare the biological effects of the aggregation process in the [*PIN*$^+$] and [*pin*$^-$] strain backgrounds. Induction of the cytosolic HSR by polyQ-expanded Htt exon 1 in yeast is regulated by Sis1 and is enhanced at elevated Sis1 levels (Klaips et al., 2020). In [*PIN*$^+$] cells, 97Q-Opto induced a stress response dependent on *SIS1* overexpression in the absence of light, similar to 97Q (Figures 4A and S4A). Illumination led to a further ~2-fold increase of HSR reporter activity (Figure 4A), consistent with enhanced aggregation upon light-induced clustering (Figure 3A). In contrast, light-induced aggregation of 97Q-Opto in [*pin*$^-$] cells did not activate the Sis1-dependent HSR (Figure 4A), although similar amounts of SDS-resistant aggregates were produced as in [*PIN*$^+$] cells in the absence of light (Figure S4B). Illumination of [*pin*$^-$] cells even tended to diminish the minor HSR that was observed with 97Q-Opto in the dark (Figure 4A). Because the [*pin*$^-$] strain is capable of mounting a normal HSR at elevated temperature (Figure 1F), with or without the presence of light-induced 97Q-Opto aggregates (Figure S4C), these results suggested a qualitative difference in polyQ aggregate properties between [*PIN*$^+$] and [*pin*$^-$] strains.

Oligomeric aggregates of polyQ expansion protein, detectable by semi-denaturing detergent agarose gel electrophoresis (SDD-AGE), were shown to bind Sis1, thereby playing a critical role in inducing the cytosolic HSR (Klaips et al., 2020). Analysis of cell lysates by SDD-AGE demonstrated the presence of distinct 97Q-Opto species in [*PIN*$^+$] cells migrating in the upper half of the gel, which we operationally defined as oligomers (Figure 4B). Light activation did not interfere with oligomer formation (Figure 4B). These 97Q-Opto oligomers were not detected in [*pin*$^-$] cells, even with light activation (Figure 4B). The oligomers in [*PIN*$^+$] cells formed in a polyQ length-dependent manner (Figure S4D) and withstood 2% SDS (present in the SDD-AGE running buffer), suggesting stabilizing interactions between polyQ sequences. They were partially soluble upon cell

(D) [*pin*$^-$] yeast cells coexpressing the proteins indicated were grown in the absence (dark) or presence (light) of blue light for 20 h. 300 μg of total lysate protein were analyzed by filtration; immunodetection with anti-mCherry (magenta) and anti-GFP (green) antibody. A representative result is shown from experiments performed in triplicate.

(E) mCherry-Opto or polyQ-Opto were integrated into the genome and expressed under the *GPD* promoter. Cells were grown either in the absence (dark) or presence (light) of blue light for 20 h. 300 μg of total lysate protein were analyzed by filter assay; immunodetection with anti-mCherry antibody. A representative result is shown from experiments performed in triplicate. *, 60 μg of total protein was loaded. Protein retained was quantified via densitometric analysis. Data represent mean + SD (n = 3).

(F) mCherry-Opto or polyQ-Opto were expressed in [*pin*$^-$] cells from 2μ plasmids under the control of a galactose-inducible promoter for ~23 h. Cells were grown either in the absence (dark) or presence (light) of blue light. Cell lysates were analyzed as in (E). A representative result from experiments performed in triplicate is shown. Data represent mean + SD (n = 3).

See also Figure S3.

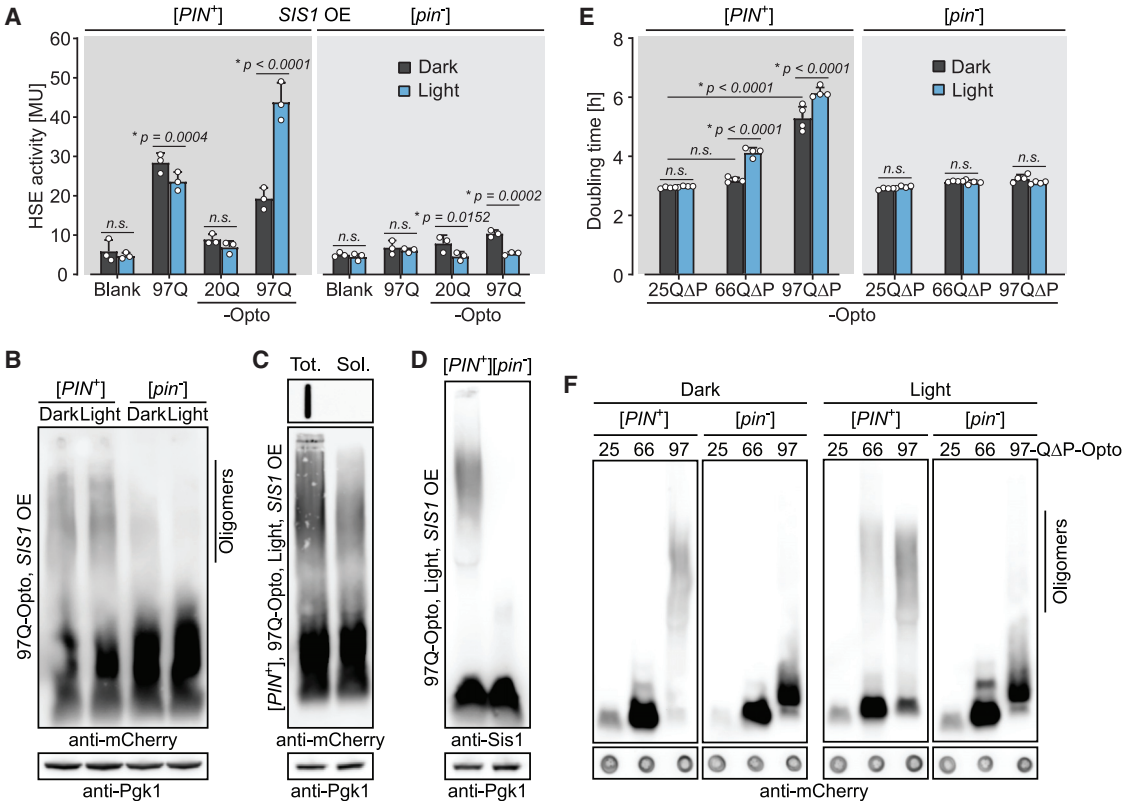

Figure 4. [*PIN*$^+$] cells accumulate polyQ oligomers

(A) Expression of polyQ-Opto proteins in [*PIN*$^+$] cells induces a Sis1-dependent HSR. β-Galactosidase activity was measured in [*PIN*$^+$] and [*pin*$^-$] cells expressing the pHSELacZ HSR reporter with *SIS1* overexpression and coexpression of empty vector or the proteins indicated from 2μ plasmids under galactose control. Cells were grown in the absence (dark) or presence (light) of blue light in inducing media for ~23 h. Data represent mean + SD (n = 3).

(B) *SIS1*-overexpressing [*PIN*$^+$] and [*pin*$^-$] cells coexpressing 97Q-Opto as in (A) were grown either in the absence (dark) or presence (light) of blue light in inducing media for ~23 h. Identical amounts of total protein from lysates were analyzed by SDD-AGE and immunodetection with anti-mCherry antibody. Analysis by SDS-PAGE and immunoblotting for Pgk1 served as loading control. Representative results are shown from experiments performed in triplicate.

(C) *SIS1*-overexpressing [*PIN*$^+$] cells coexpressing 97Q-Opto as in (A) were grown in blue light and inducing media for ~23 h. Lysate was separated into total (Tot.) and soluble (Sol.) fractions by centrifugation (15,000 × *g*). Samples were analyzed by filtration (top) or SDD-AGE (bottom), followed by immunodetection with anti-mCherry antibody. SDS-PAGE and immunoblotting for Pgk1 served as loading control. Representative results are shown from experiments performed in triplicate.

(D) Selected samples from (B) were analyzed by SDD-AGE and immunodetection with anti-Sis1 antibody. Representative results are shown from experiments performed in triplicate.

(E) [*PIN*$^+$] or [*pin*$^-$] cells expressing the indicated ΔP-Opto proteins from 2μ plasmids under a galactose-inducible promoter were grown in the absence (dark) or presence (light) of blue light in inducing media for ~40 h. Subsequently, OD_{600} was measured in log phase cultures over the course of 8 h and doubling times were calculated. Data represent mean + SD (n = 4).

(F) Lysates of [*PIN*$^+$] or [*pin*$^-$] cells expressing ΔP-Opto proteins as in (E) for ~48 h were analyzed by SDD-AGE. Lysates were normalized to equal amounts of polyQΔP-Opto, with dot blot analysis (lower panel) serving as a loading control. Membranes were processed for immunodetection with anti-mCherry antibody. Representative results are shown from experiments performed in triplicate.

See also Figure S4.

fractionation, in contrast to the polyQ protein in large, SDS-resistant inclusions, which were completely excluded from the supernatant fraction (Figure 4C). As Sis1 binding to oligomer species is critical for induction of the HSR (Klaips et al., 2020), the apparent absence of Sis1-binding oligomers can explain the lack of a HSR in the [*pin*$^-$] strain (Figure 4D).

Expression of polyQ-expanded Htt exon 1 does not cause overt toxicity in yeast. However, variants of exon 1 lacking large parts of the 52 amino acid poly-proline region following the polyQ tract (Figure 2A) are toxic in [*PIN*$^+$] cells, causing a pronounced polyQ length-dependent growth defect (Dehay and Bertolotti, 2006; Duennwald et al., 2006a, 2006b). To test whether optogenetic aggregation can circumvent the prion requirement for polyQ toxicity, we expressed polyQΔP-Opto proteins with increasing polyQ lengths (Figure 4E). [*PIN*$^+$] cells expressing 97QΔP-Opto in the absence of light grew significantly more slowly than 25QΔP-Opto control cells (Figure 4E). Constant light exposure further slowed cell growth upon 97QΔP-Opto expression (Figure 4E). Light activation also lowered the polyQ length threshold for growth inhibition to 66 Q (Figure 4E). The protein levels of

polyQΔP-Opto in [*PIN*$^+$] cells correlated inversely with toxicity, as cells are under selection pressure for low expression levels of toxic species (Figure S4E). Consequently, light activation of aggregation of 66QΔP-Opto, causing growth inhibition, resulted in reduced expression of this construct (Figure S4E). Note that expression levels of soluble 25QΔP-Opto were generally low, presumably due to more rapid turnover in the absence of aggregation. In contrast, light induction of polyQΔP-Opto proteins in [*pin*$^-$] cells did not result in toxicity, as reflected by the absence of a growth defect (Figure 4E). Consistently, in the absence of toxic effects, the expression levels of polyQΔP-Opto proteins in [*pin*$^-$] cells were higher than in the [*PIN*$^+$] strain (Figure S4E).

Interestingly, the extent of growth inhibition caused by the polyQΔP-Opto proteins in [*PIN*$^+$] cells correlated with the abundance of oligomeric aggregates by SDD-AGE, with light induction resulting in the appearance of oligomers at the 66 Q toxicity threshold (Figure 4F). In contrast, no polyQΔP-Opto oligomers accumulated in [*pin*$^-$] cells, with or without light activation (Figure 4F). Instead of oligomeric species, light activated [*pin*$^-$] cells accumulated larger amounts of insoluble, SDS-resistant polyQΔP-Opto aggregates than [*PIN*$^+$] cells (Figure S4F), supporting the conclusion that the insoluble inclusions are not the primary toxic species. Although in [*PIN*$^+$] cells 66QΔP-Opto formed large SDS-resistant aggregates in both the absence and presence of light, toxic effects were only observed upon appearance of oligomers under light activation (Figures 4E, 4F, and S4F). Thus, toxic effects are mediated by polyQ oligomers rather than insoluble inclusions.

Taken together, the [*PIN*$^+$] prion status modulates polyQ aggregation, resulting in the accumulation of toxic polyQ oligomers. This effect is prion-specific, as it cannot be recreated in the [*pin*$^-$] strain by light-induced clustering of polyQ proteins.

PolyQ oligomers form by templating on Rnq1 prions

The [*PIN*$^+$] prion may modulate polyQ aggregation directly or indirectly. Given the [*PIN*$^+$] dependence of polyQ oligomer formation described above, a direct effect would imply an interaction between soluble polyQ species and Rnq1 prions. To test this possibility, we analyzed the interactome of total and soluble 97Q-Opto in [*PIN*$^+$] cells relative to [*pin*$^-$] cells, with and without light activation, by 97Q-Opto pull-down and label-free proteomics (Figure 5A). 212 proteins were significantly enriched by pull-down of 97Q-Opto from [*PIN*$^+$] total lysate ($\geq$1.5-fold relative to [*pin*$^-$]; $p < 0.05$), which we defined as interactors (Figure S5A; Table S4). Among the most highly enriched interactors (2- to 70-fold) were the prions Rnq1, Pin3, and Sup35, as well as the proteins Gts1, Sgt2, and Sis1, which have been classified as prion-like based on the presence of characteristic LCRs (Alberti et al., 2009) (Figure S5A; Table S4). The number of interactors increased to 453 when aggregation was enhanced by illumination (Figure S5B; Table S4). These findings are in agreement with reports that polyQ aggregates in yeast and mammalian cells interact with and sequester prion-like proteins and other factors, including proteostasis components (Kim et al., 2016; Park et al., 2013; Ripaud et al., 2014). These interactions are dependent on the [*PIN*$^+$] prion state.

In contrast to the large number of polyQ interactors identified in total lysates, the interactome of soluble polyQ species (supernatant after centrifugation at 15,000 × *g*) was more limited. We identified 62 interactors as significantly enriched on soluble 97Q-Opto in the [*PIN*$^+$] condition (Figure 5B; Table S4), with only a moderate increase to 74 interactors with additional light activation of aggregation (Figure 5C; Table S4). Many interactors of soluble 97Q-Opto were also identified in the total 97Q-Opto interactome of [*PIN*$^+$] cells (Figure 5D), including Rnq1, Pin3, and Sis1 (Figures 5B–5D). Strikingly, Rnq1 was at least ~10-fold more enriched in the soluble 97Q-Opto interactome and ~10- to 100-fold more abundant (based on intensity based absolute quantification, iBAQ (Schwanhäusser et al., 2011)) than the other prion-like proteins, reaching a molar ratio of Rnq1 to polyQ of ~1:5 (Figure 5E; Table S4).

To further explore a direct effect of Rnq1 prions on polyQ aggregation, we performed *in vitro* aggregation experiments with purified, recombinant Htt exon 1 containing 54 Q (Htt54Q). Aggregation was initiated by cleavage of Htt54Q from a glutathione *S*-transferase (GST) solubility tag at an engineered protease site (Muchowski et al., 2000; Scherzinger et al., 1997) (Figure 6A). Note that longer polyQ tracts are difficult to produce recombinantly (Scherzinger et al., 1997). Htt54Q, but not Htt20Q, readily formed SDS-resistant aggregates, as detected by filter assay (0.2 μm pore size) (Muchowski et al., 2000; Scherzinger et al., 1997) (Figures S6A and S6B). When aggregation was performed in the presence of lysate from [*pin*$^-$] or [*PIN*$^+$] cells (4.4 mg total protein/mL), formation of SDS-resistant aggregates was substantially inhibited (Figure 6B), consistent with the presence of strong anti-aggregation activities in both strains. This inhibition was not caused by a nonspecific protein effect (Figure S6C) and was not due to interference with the proteolytic cleavage of GST-polyQ (Figure S6D).

Oligomers of Htt54Q were not detected by SDD-AGE during aggregation in the presence of [*PIN*$^+$] cell lysate (Figure S6E), suggesting the possibility that the concentration of Rnq1 prions in the *in vitro* reaction (~45-fold diluted compared with cellular concentration) was too low to produce the effects observed *in vivo*. As this dilution is technically unavoidable, we overexpressed *RNQ1-GFP* in [*pin*$^-$] and [*PIN*$^+$] cells to more closely approach the physiological Rnq1 concentration. As shown above, Rnq1-GFP forms prion aggregates in the [*PIN*$^+$] strain and is soluble in [*pin*$^-$] cells (Figure S1B). Addition of lysate from *RNQ1-GFP*-expressing [*PIN*$^+$] cells, but not *RNQ1-GFP*-expressing [*pin*$^-$] cells, robustly induced the formation of polyQ oligomers during *in vitro* aggregation (Figures 6C and 6D), recapitulating the observations *in vivo*. In addition, larger aggregates of Htt54Q accumulated at the top of the SDD-AGE gel in the presence of [*PIN*$^+$] lysate (Figures 6C and 6D), while the formation of SDS-resistant aggregates >0.2 μm, detected by filter assay, was only mildly enhanced compared with reactions containing [*pin*$^-$] lysate (Figure 6C). Importantly, polyQ oligomers accumulated at the expense of monomer (Figure 6C), suggesting that the Rnq1 prion plays an active role in oligomer production. These species were kinetically stable and co-existed with larger aggregates. Immunoblotting for Rnq1-GFP revealed the presence of Rnq1-GFP prion aggregates specifically in [*PIN*$^+$] reactions, comigrating with the Htt54Q oligomers (Figure 6D). However, the migration of the Rnq1 prions was independent of the presence of polyQ oligomers, suggesting that the two forms of

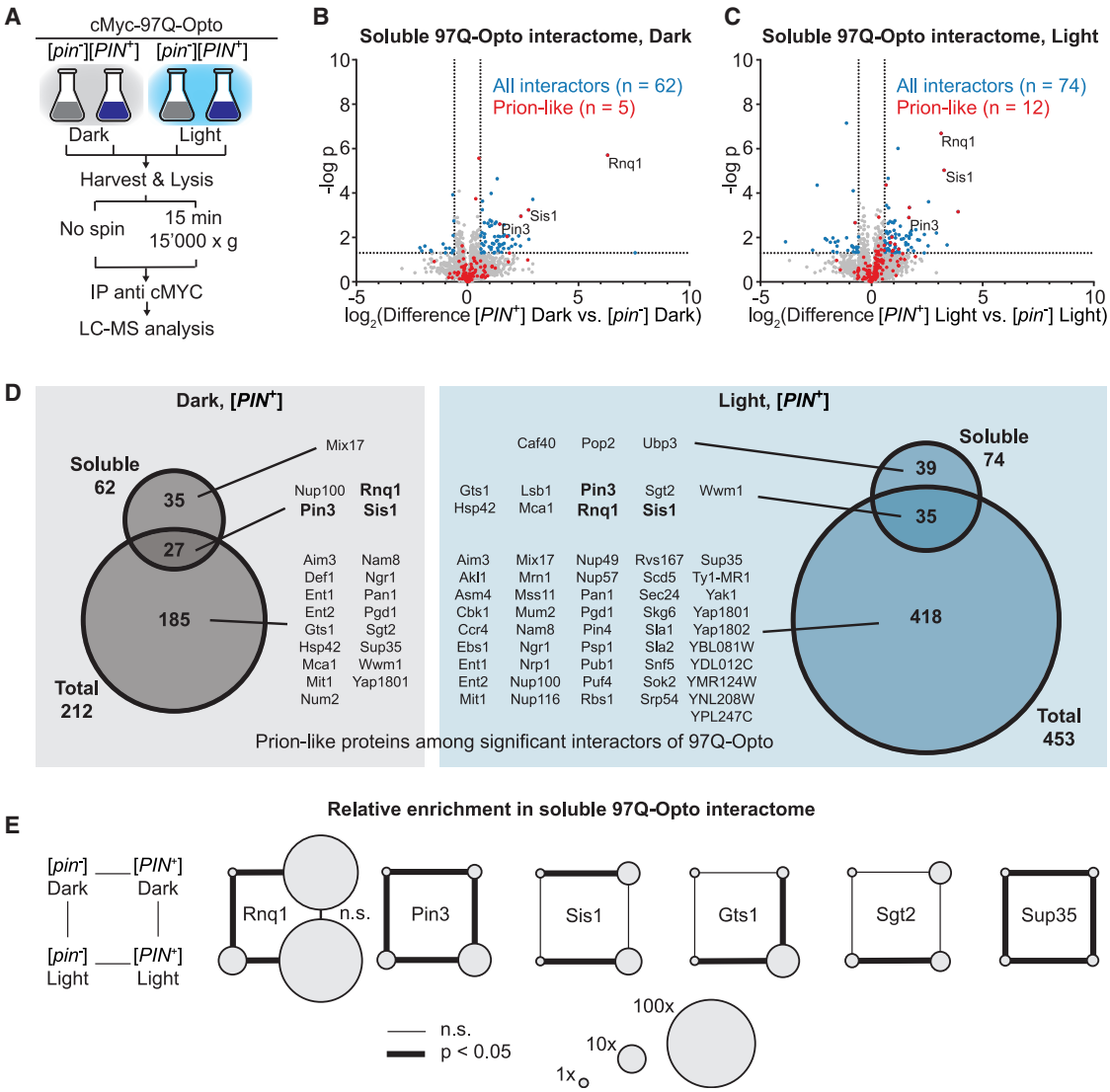

Figure 5. [*PIN*$^+$]-dependent interaction of 97Q-Opto with Rnq1

(A) 97Q-Opto interactome analysis. [*PIN*$^+$] and [*pin*$^-$] cells expressing cMyc-tagged 97Q-Opto from an integrated endogenous locus under the *GPD* promoter were grown in the absence (dark) or presence (light) of blue light for 20 h prior to cell harvest and lysis. Total lysate and soluble fraction were subjected to anti-cMyc IP, followed by label-free mass spectrometry.

(B and C) Volcano plot representations of label-free interactome analysis of 97Q-Opto after anti-cMyc IP from soluble lysate fractions of [*PIN*$^+$] and [*pin*$^-$] cells grown in the absence (B) or presence (C) of blue light (n = 4). Significantly enriched proteins (≥1.5-fold, $p < 0.05$) are marked in blue, prion-like proteins in red. Selected interactors are annotated.

(D) Overlap of interactors of soluble (top circles, related to Figures 5B and 5C) or total (bottom circles, related to Figures S5A and S5B) 97Q-Opto in [*PIN*$^+$] in the absence (dark, left) or presence (light, right) of blue light. Prion-like interactors are annotated.

(E) Schematic representation of the relative enrichment of selected prion-like proteins in the interactomes of soluble 97Q-Opto in the conditions indicated (related to Figures 5B and 5C). Data based on 4 independent experiments. Bold connecting line between conditions indicates significance ($p < 0.05$), area of circle represents enrichment normalized to the least enriched condition for each protein.

See also Figure S5 and Table S4.

aggregate did not stably interact during SDD-AGE. This is consistent with Rnq1 prions acting as a catalytic template for the formation polyQ oligomers.

To obtain further insight into the prion mechanism of polyQ oligomer formation, we immobilized Rnq1-GFP prion aggregates from [*PIN*$^+$] cells on anti-GFP beads and added the beads to polyQ aggregation reactions in [*pin*$^-$] lysate (Figure 6E). Rnq1-GFP from [*pin*$^-$] cells bound to beads served as control. The immobilized Rnq1-GFP prions, but not the non-prion Rnq1-GFP, induced the efficient formation of Htt54Q oligomers (Figures 6F and S6F), with oligomer levels reaching a plateau after ~10 h of incubation with prion beads (Figure S6F). Importantly, the

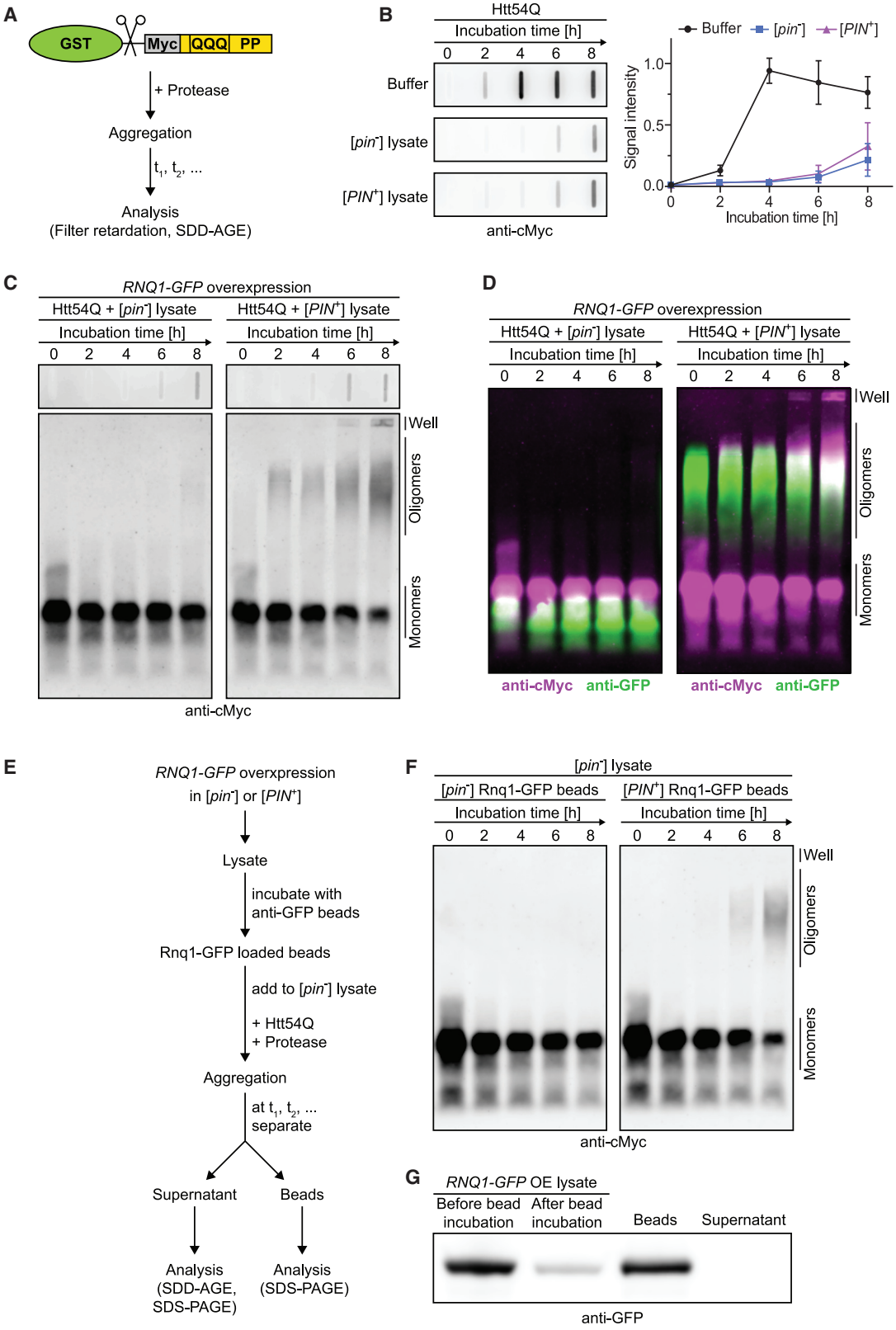

(legend on next page)

Rnq1-GFP prions remained bound to the beads and could be removed from the aggregation reaction by centrifugation, while the polyQ oligomers stayed soluble in the absence of detectable prion (Figures 6F and 6G), confirming the transient nature of the interaction.

Taken together, Rnq1 prions transiently interact with soluble polyQ protein to mediate the accumulation of polyQ oligomers, which are then responsible for downstream biological effects.

DISCUSSION

The yeast *S. cerevisiae* has served as a valuable model system in studies of polyQ protein aggregation associated with HD (Duennwald, 2011; Khurana and Lindquist, 2010). To understand how specific cellular backgrounds facilitate aggregate pathology, we took advantage of the [*PIN*$^+$] prion dependence of polyQ protein aggregation and toxicity in yeast. We used an optogenetic strategy to circumvent the prion requirement and induced the aggregation of polyQ-expanded Htt exon 1 in prion-free [*pin*$^-$] cells. The light-induced polyQ-Opto aggregates replicated basic structural and functional features of the polyQ inclusions formed in the [*PIN*$^+$] strain (Figure 7A). However, the optogenetic aggregation pathway in [*pin*$^-$] cells was not associated with toxicity or other cellular effects; it bypassed the formation of soluble oligomeric polyQ species, which accumulated exclusively in the [*PIN*$^+$] strain and were responsible for cell toxicity (Figure 7B). *In vitro* reconstitution experiments supported a model in which polyQ oligomers are generated through a heterologous templating mechanism on Rnq1 prions. These findings provide a mechanistic explanation for the prion dependence of polyQ aggregation and toxicity in the yeast system and suggest that prion-like proteins may have a similar role in disease manifestation in humans.

Rnq1 prions induce toxic polyQ oligomers

Aggregation of polyQ expansion proteins is thought to be a multistep process (Ossato et al., 2010; Vitalis and Pappu, 2011), involving the local clustering of monomers through condensate formation (Peskett et al., 2018), followed by the stochastic formation of critical aggregation nuclei (Chen et al., 2002; Sinnige et al., 2021; Walters and Murphy, 2011; Yushchenko et al., 2018). Consistent with such a mechanism, we triggered aggregation in [*pin*$^-$] yeast by light-induced clustering of polyQ-Opto protein, resulting in a high local concentration of expanded polyQ sequences and thereby increasing the probability of primary nucleation events (Figure 7A). Indeed, high level overexpression of polyQ-Opto (in the absence of light) was sufficient to allow aggregation even in [*pin*$^-$] cells, albeit at low efficiency (Figure 3F). In contrast, in the [*PIN*$^+$] background, the critical polyQ concentration for aggregation is dramatically reduced compared with [*pin*$^-$] cells. However, we found both strains to have comparable proteostasis capacity, arguing against an indirect effect of the prion in mediating polyQ aggregation. As demonstrated *in vivo* and upon reconstitution *in vitro*, Rnq1 prions interact transiently with soluble polyQ molecules, cross-seeding aggregation and resulting in the production of soluble polyQ oligomers (Figure 7B). The prion acts catalytically in this process, as it can be removed from the aggregation reaction, leaving soluble polyQ oligomers. These oligomers are responsible for the toxic polyQ effects observable in the [*PIN*$^+$] strain, providing independent evidence for the central role of oligomers as toxic species (Arrasate et al., 2004; Behrends et al., 2006; Haass and Selkoe, 2007; Kayed et al., 2003; Kim et al., 2016; Klaips et al., 2020; Leitman et al., 2013; Takahashi et al., 2008). While Rnq1 was by far the most abundant prion associated with soluble polyQ species, other prions also interact and may participate in oligomer formation. These prions, including Sup35 [*PSI*$^+$], also form in a manner dependent on the [*PIN*$^+$] state (Serio, 2018), suggesting a similar mechanism of cross-seeding by Rnq1 prions. The polyQ oligomers generated by prion-mediated nucleation are stable under the conditions of SDD-AGE electrophoresis in the presence of SDS and thus may contain amyloid-like structural elements. They appear to be separated from end-state insoluble aggregates by a substantial kinetic energy barrier, resulting in the accumulation of large amounts of toxic species.

Figure 6. PolyQ oligomers form through direct interaction with Rnq1 prions

(A) Htt54Q aggregation was initiated by proteolytic cleavage of GST-cMycHtt54Q. After different times, reactions were analyzed by filter assay or SDD-AGE, followed by anti-cMyc immunodetection.

(B) Aggregation reactions were performed in the presence of *in vitro* reaction buffer or buffer with total lysate from [*pin*$^-$] or [*PIN*$^+$] cells (4.4 mg total protein/mL). Analysis by filter assay and immunodetection with anti-cMyc antibody is shown. Aggregation reactions were quantified by densitometry. Data represents mean ± SD (n = 3).

(C) Aggregation reactions were performed in the presence of cell lysate (4.4 mg total protein/mL) from [*pin*$^-$] or [*PIN*$^+$] cells overexpressing *RNQ1-GFP*. Analysis by filter assay (top panels) and SDD-AGE (bottom panels), followed by anti-cMyc immunodetection is shown. Representative results are shown from experiments performed in triplicate.

(D) Immunoblots of SDD-AGE gels shown in (C) were additionally processed for detection of Rnq1-GFP with anti-GFP antibody. Signals from anti-cMyc (magenta) and anti-GFP (green) are overlaid. A representative result is shown from experiments performed in triplicate.

(E) *In vitro* aggregation reactions in the presence of Rnq1-GFP immobilized on beads. Anti-GFP beads were added to lysate of [*pin*$^-$] or [*PIN*$^+$] cells overexpressing *RNQ1-GFP* and incubated overnight. Rnq1-GFP-loaded beads were isolated and mixed with [*pin*$^-$] cell lysate. Htt54Q aggregation reactions were performed in this suspension as described in (A). At different time points, supernatant was separated from beads by centrifugation and samples were analyzed by SDD-AGE (see Figures 6F and S6F) and SDS-PAGE (see Figure 6G).

(F) Aggregation reactions were performed in [*pin*$^-$] cell lysate (4.4 mg total protein/mL) in the presence of Rnq1-GFP-loaded beads from [*pin*$^-$] or [*PIN*$^+$] cells overexpressing *RNQ1-GFP*. Analysis by SDD-AGE, followed by immunodetection with anti-cMyc antibody. A representative result is shown from experiments performed in triplicate.

(G) Samples taken at different stages of the experiment in (E) were analyzed for Rnq1-GFP prions by SDS-PAGE and anti-GFP immunodetection. Rnq1-GFP amounts loaded are directly comparable. A representative result from experiments performed in triplicate is shown.

See also Figure S6.

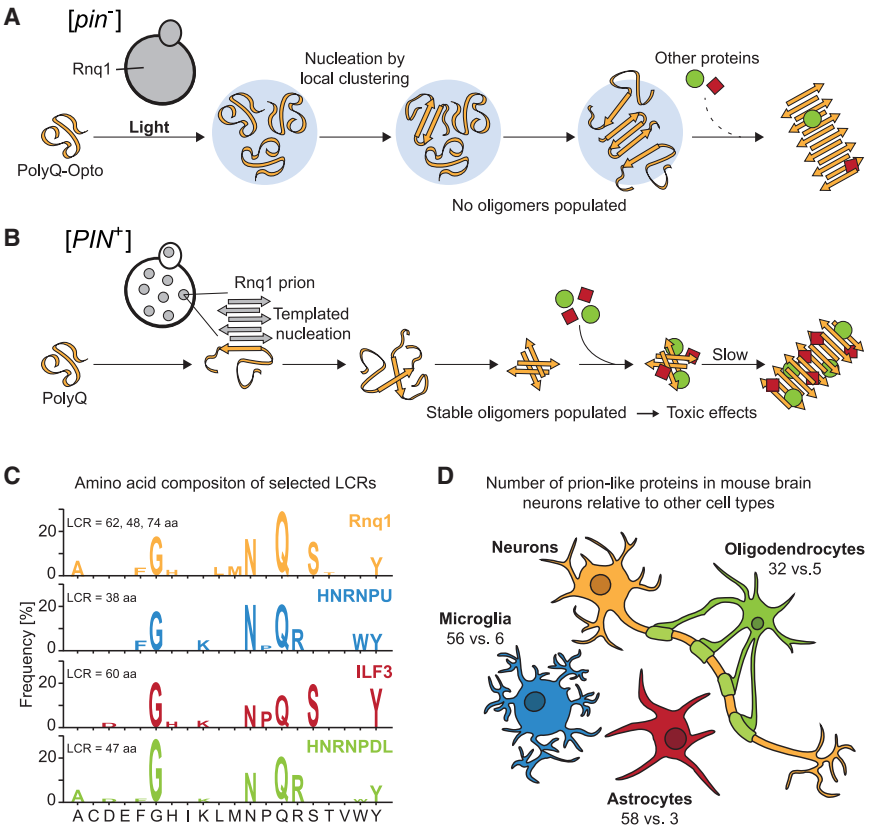

Figure 7. Model of prion effects on polyQ protein aggregation

(A) Optogenetic aggregation in [*pin*⁻] cells. Light-induced condensate formation of polyQ-Opto monomers facilitates aggregate nucleation of locally clustered polyQ sequences and leads to formation of SDS-resistant aggregates. Soluble polyQ oligomers do not accumulate.

(B) Aggregation in [*PIN*⁺] cells. Soluble polyQ protein (monomer or reversible oligomer) interacts with Rnq1 prions, which offer a surface for heterologous templating and nucleation of polyQ oligomers that are stabilized (SDS-resistant) by interactions between polyQ sequences. These oligomers engage in aberrant interactions with multiple endogenous proteins, resulting in toxic effects reflected in growth inhibition and induction of the cytosolic HSR. They convert slowly to large, insoluble aggregates.

(C) Amino acid composition of LCRs of yeast Rnq1 and mammalian interactors of soluble polyQ, HNRNPU, ILF3, and HNRNPDL. LCRs were identified using the SEG algorithm (Wootton and Federhen, 1993). For Rnq1 the average composition of the three LCRs located in the prion domain is shown. Lengths of LCRs are indicated.

(D) Proteome analysis from Sharma et al. (2015) indicating the number of enriched prion-like proteins identified in neurons extracted from mouse brain in comparison with astrocytes, microglia, and oligodendrocytes.

Possible implications for neurodegenerative pathology

Our findings lead us to hypothesize that the prion dependence of polyQ aggregation and toxicity is not an idiosyncrasy of yeast but rather may reflect a more general principle with relevance in the neuronal system as well. How can this possibility be reconciled with the widely held view that an age-dependent decline in general proteostasis capacity is critical in facilitating the manifestation of polyQ pathologies and other neurodegenerative diseases associated with protein aggregation (Douglas and Dillin, 2010; Hipp et al., 2014; Klaips et al., 2018; Labbadia and Morimoto, 2015)? Specifically, it has been shown in the nematode model that taxing the proteostasis system by expressing misfolding proteins can enhance polyQ aggregation and shift the aggregation threshold to shorter polyQ lengths (Gidalevitz et al., 2006). We suggest that diminishing proteostasis capacity leads to the accumulation of LCR-containing, prion-like aggregates in neurons, which trigger polyQ aggregate nucleation by cross-templating, specifically inducing the accumulation of toxic polyQ oligomers. Similar processes may play a role in the manifestation of other age-dependent neurodegenerative syndromes. In this proposed model, prion-like aggregates of multiple endogenous proteins function as drivers of pathologically relevant effects of age-dependent proteostasis decline.

These considerations are compatible with available data resources on proteins with prion-like LCRs in mammalian cells and model organisms (Espinosa Angarica et al., 2014; Harel et al., 2022; Iglesias et al., 2019; Kim et al., 2016; March et al., 2016; Walther et al., 2015), proteins with a high propensity to undergo phase separation and amyloid-like aggregation (Hardenberg et al., 2020; Kato et al., 2012; Sprunger and Jackrel, 2021; Vecchi et al., 2020; Zbinden et al., 2020). The interactome of soluble oligomeric species of polyQ-expanded Huntingtin in mammalian cells shows a significant enrichment of prion-like, LCR-containing proteins (Kim et al., 2016), including the proteins TDP43 and FUS, which are associated with other neurodegenerative pathologies (Chen-Plotkin et al., 2010; Deng et al., 2014; Zbinden et al., 2020). The LCRs of several of these proteins closely resemble the prion domain of yeast Rnq1 in terms of amino acid composition, being rich in glutamine, asparagine, and glycine (Figure 7C). Neurons are known to be particularly sensitive to pathological protein aggregation (Fu et al., 2018). Indeed, proteomic analyses of primary cultured mouse brain cells and corresponding brain tissue samples revealed a pronounced enrichment of aggregation-prone, prion-like proteins in neurons compared with other brain cell types (Sharma et al., 2015) (Figure 7D). Importantly, such prion-like proteins show a strong age-dependent increase in aggregation, as observed in *C. elegans* (Vecchi et al., 2020; Walther et al., 2015) and in the aging vertebrate brain (Harel et al., 2022). Furthermore, the age-dependent accumulation of distinct prion-like aggregates in certain brain regions could explain their preferential vulnerability to specific neurodegenerative disease proteins (Brettschneider et al., 2015; Fu et al., 2018).

While major efforts in developing therapeutics are focused on preventing the amyloid-like aggregation of specific disease proteins, we suggest that reducing general age-dependent aggregation by boosting proteostasis holds great promise in delaying neurodegenerative pathologies.

Limitations of the study

Our results support a model in which Rnq1 prions are directly promoting the formation of biologically active polyQ oligomers in a catalytic templating mechanism. How exactly the prion acts in this process remains to be investigated further. For example, we cannot rule out that polyQ oligomers form spontaneously, but in the absence of prion are either reversible or convert rapidly to larger aggregates, preventing toxic polyQ effects. In this scenario, the interaction with prion would impart structural information that generates kinetically stable oligomers. Such a mechanism would likely involve a structural rearrangement at the prion surface and/or the inclusion of small amounts of prion into the oligomers. We note, however, that Rnq1 prions bound to beads could be efficiently removed from aggregation reactions without depleting oligomers (Figures 6F and 6G).

Although previous reports and resource data provide support for a role of prion-like proteins in cross-seeding pathological protein aggregation, such a mechanism remains speculative at this point.

STAR★METHODS

Detailed methods are provided in the online version of this paper and include the following:

- KEY RESOURCES TABLE
- RESOURCE AVAILABILITY
  - Lead contact
  - Materials availability
  - Data and code availability
- EXPERIMENTAL MODEL AND SUBJECT DETAILS
- METHOD DETAILS
  - Molecular cloning
  - Yeast strains
  - General sample handling
  - Preparation of cell extracts
  - Mass spectrometry
  - Cycloheximide chase
  - Alkaline lysis and TCA precipitation
  - SDS-PAGE
  - SDD-AGE
  - Immunoblotting
  - β-Galactosidase activity assay
  - Confocal imaging
  - Filter retardation assay
  - Cell fractionation
  - Growth assay
  - FACS analysis
  - Recombinant protein expression
  - Recombinant protein purification
  - *In vitro* aggregation assay
- QUANTIFICATION AND STATISTICAL ANALYSIS

SUPPLEMENTAL INFORMATION

Supplemental information can be found online at https://doi.org/10.1016/j.molcel.2022.09.031.

ACKNOWLEDGMENTS

We thank Clifford Brangwynne (Princeton University, USA) for providing plasmids. Silvia Gärtner, Romy Lange, and Nadine Wischnewski are acknowledged for expert technical assistance. We thank the staff of the MPIB core facility for competent technical support with MS experiments. We thank Cole Sitron for critically reading the manuscript and Michele Vendruscolo for discussion. The research leading to these results has received funding from the Deutsche Forschungsgemeinschaft (DFG, German Research Foundation) under Germany's Excellence Strategy within the framework of the Munich Cluster for Systems Neurology (EXC 2145 SyNergy—ID 390857198) (F.U.H.). M.H.M.G. was supported by a DFG fellowship through the Graduate School of Quantitative Biosciences Munich (QBM). C.L.K. acknowledges funding by the Alexander von Humboldt Foundation (Postdoctoral Fellowship 3.1-USA/1162753 HFST-P).

AUTHOR CONTRIBUTIONS

M.H.M.G. planned and performed all experiments and analyzed the data. F.U.H. conceived the project and participated in data interpretation together with the other authors. C.L.K. acted as co-supervisor. M.H.M.G., C.L.K., and F.U.H. wrote the paper.

DECLARATION OF INTERESTS

F.U.H. is a member of the *Molecular Cell* advisory board.

INCLUSION AND DIVERSITY

One or more of the authors of this paper self-identifies as a member of the LGBTQ+ community.

Received: April 27, 2022
Revised: August 22, 2022
Accepted: September 28, 2022
Published: October 21, 2022

REFERENCES

Alberti, S., Halfmann, R., King, O., Kapila, A., and Lindquist, S. (2009). A systematic survey identifies prions and illuminates sequence features of prionogenic proteins. Cell *137*, 146–158. https://doi.org/10.1016/j.cell.2009.02.044.

Anckar, J., and Sistonen, L. (2011). Regulation of HSF1 function in the heat stress response: implications in aging and disease. Annu. Rev. Biochem. *80*, 1089–1115. https://doi.org/10.1146/annurev-biochem-060809-095203.

Arrasate, M., Mitra, S., Schweitzer, E.S., Segal, M.R., and Finkbeiner, S. (2004). Inclusion body formation reduces levels of mutant huntingtin and the risk of neuronal death. Nature *431*, 805–810. https://doi.org/10.1038/nature02998.

Ashburner, M., Ball, C.A., Blake, J.A., Botstein, D., Butler, H., Cherry, J.M., Davis, A.P., Dolinski, K., Dwight, S.S., Eppig, J.T., et al. (2000). Gene ontology: tool for the unification of biology. Nat. Genet. *25*, 25–29. https://doi.org/10.1038/75556.

Bähler, J., Wu, J.-Q., Longtine, M.S., Shah, N.G., McKenzie, A., III, Steever, A.B., Wach, A., Philippsen, P., and Pringle, J.R. (1998). Heterologous modules for efficient and versatile PCR-based gene targeting in *Schizosaccharomyces pombe*. Yeast *14*, 943–951. https://doi.org/10.1002/(SICI)1097-0061(199807)14:10<943::AID-YEA292>3.0.CO;2-Y.

Balch, W.E., Morimoto, R.I., Dillin, A., and Kelly, J.W. (2008). Adapting proteostasis for disease intervention. Science *319*, 916–919. https://doi.org/10.1126/science.1141448.

Bäuerlein, F.J.B., Saha, I., Mishra, A., Kalemanov, M., Martínez-Sánchez, A., Klein, R., Dudanova, I., Hipp, M.S., Hartl, F.U., Baumeister, W., and Fernandez-Busnadiego, R. (2017). *In situ* architecture and cellular interactions of polyQ Inclusions. Cell *171*, 179–187.e10. https://doi.org/10.1016/j.cell.2017.08.009.

Behrends, C., Langer, C.A., Boteva, R., Böttcher, U.M., Stemp, M.J., Schaffar, G., Rao, B.V., Giese, A., Kretzschmar, H., Siegers, K., and Hartl, F.U. (2006). Chaperonin TRiC promotes the assembly of polyQ expansion proteins into nontoxic oligomers. Mol. Cell *23*, 887–897. https://doi.org/10.1016/j.molcel.2006.08.017.

Bradley, M.E., Edskes, H.K., Hong, J.Y., Wickner, R.B., and Liebman, S.W. (2002). Interactions among prions and prion "strains" in yeast. Proc. Natl. Acad. Sci. USA *99*, 16392–16399. https://doi.org/10.1073/pnas.152330699.

Brettschneider, J., Del Tredici, K., Lee, V.M., and Trojanowski, J.Q. (2015). Spreading of pathology in neurodegenerative diseases: a focus on human studies. Nat. Rev. Neurosci. *16*, 109–120. https://doi.org/10.1038/nrn3887.

Bugaj, L.J., Choksi, A.T., Mesuda, C.K., Kane, R.S., and Schaffer, D.V. (2013). Optogenetic protein clustering and signaling activation in mammalian cells. Nat. Methods *10*, 249–252. https://doi.org/10.1038/nmeth.2360.

Chen, S., Berthelier, V., Yang, W., and Wetzel, R. (2001). Polyglutamine aggregation behavior in vitro supports a recruitment mechanism of cytotoxicity. J. Mol. Biol. *311*, 173–182. https://doi.org/10.1006/jmbi.2001.4850.

Chen, S., Ferrone, F.A., and Wetzel, R. (2002). Huntington's disease age-of-onset linked to polyglutamine aggregation nucleation. Proc. Natl. Acad. Sci. USA *99*, 11884–11889. https://doi.org/10.1073/pnas.182276099.

Chen-Plotkin, A.S., Lee, V.M., and Trojanowski, J.Q. (2010). TAR DNA-binding protein 43 in neurodegenerative disease. Nat. Rev. Neurol. *6*, 211–220. https://doi.org/10.1038/nrneurol.2010.18.

Chernoff, Y.O., Lindquist, S.L., Ono, B., Inge-Vechtomov, S.G., and Liebman, S.W. (1995). Role of the chaperone protein Hsp104 in propagation of the yeast prion-like factor [PSI+]. Science *268*, 880–884. https://doi.org/10.1126/science.7754373.

Chiti, F., and Dobson, C.M. (2017). Protein misfolding, amyloid formation, and human disease: a summary of progress over the last decade. Annu. Rev. Biochem. *86*, 27–68. https://doi.org/10.1146/annurev-biochem-061516-045115.

Christianson, T.W., Sikorski, R.S., Dante, M., Shero, J.H., and Hieter, P. (1992). Multifunctional yeast high-copy-number shuttle vectors. Gene *110*, 119–122. https://doi.org/10.1016/0378-1119(92)90454-W.

Cox, B.S., Byrne, L.J., and Tuite, M.F. (2007). Prion stability. Prion *1*, 170–178. https://doi.org/10.4161/pri.1.3.4839.

Cox, J., and Mann, M. (2008). MaxQuant enables high peptide identification rates, individualized p.p.b.-range mass accuracies and proteome-wide protein quantification. Nat. Biotechnol. *26*, 1367–1372. https://doi.org/10.1038/nbt.1511.

De Vos, A., Anandhakumar, J., Van den Brande, J., Verduyckt, M., Franssens, V., Winderickx, J., and Swinnen, E. (2011). Yeast as a model system to study Tau biology. Int. J. Alzheimers Dis. *2011*, 428970. https://doi.org/10.4061/2011/428970.

Dehay, B., and Bertolotti, A. (2006). Critical role of the proline-rich region in huntingtin for aggregation and cytotoxicity in yeast. J. Biol. Chem. *281*, 35608–35615. https://doi.org/10.1074/jbc.M605558200.

Deng, H., Gao, K., and Jankovic, J. (2014). The role of FUS gene variants in neurodegenerative diseases. Nat. Rev. Neurol. *10*, 337–348. https://doi.org/10.1038/nrneurol.2014.78.

Derkatch, I.L., Bradley, M.E., Zhou, P., Chernoff, Y.O., and Liebman, S.W. (1997). Genetic and environmental factors affecting the *de novo* appearance of the [PSI+] prion in *Saccharomyces cerevisiae*. Genetics *147*, 507–519. https://doi.org/10.1093/genetics/147.2.507.

Derkatch, I.L., Bradley, M.E., Hong, J.Y., and Liebman, S.W. (2001). Prions affect the appearance of other prions: the story of [PIN+]. Cell *106*, 171–182. https://doi.org/10.1016/s0092-8674(01)00427-5.

Derkatch, I.L., Uptain, S.M., Outeiro, T.F., Krishnan, R., Lindquist, S.L., and Liebman, S.W. (2004). Effects of Q/N-rich, polyQ, and non-polyQ amyloids on the *de novo* formation of the [PSI+] prion in yeast and aggregation of Sup35 in vitro. Proc. Natl. Acad. Sci. USA *101*, 12934–12939. https://doi.org/10.1073/pnas.0404968101.

Di Gregorio, S.E., and Duennwald, M.L. (2018). Yeast as a model to study protein misfolding in aged cells. FEMS Yeast Res. *18*, foy054. https://doi.org/10.1093/femsyr/foy054.

Douglas, P.M., and Dillin, A. (2010). Protein homeostasis and aging in neurodegeneration. J. Cell Biol. *190*, 719–729. https://doi.org/10.1083/jcb.201005144.

Douglas, P.M., Treusch, S., Ren, H.Y., Halfmann, R., Duennwald, M.L., Lindquist, S., and Cyr, D.M. (2008). Chaperone-dependent amyloid assembly protects cells from prion toxicity. Proc. Natl. Acad. Sci. USA *105*, 7206–7211. https://doi.org/10.1073/pnas.0802593105.

Duan, L., Hope, J., Ong, Q., Lou, H.Y., Kim, N., McCarthy, C., Acero, V., Lin, M.Z., and Cui, B. (2017). Understanding CRY2 interactions for optical control of intracellular signaling. Nat. Commun. *8*, 547. https://doi.org/10.1038/s41467-017-00648-8.

Duennwald, M.L. (2011). Polyglutamine misfolding in yeast: toxic and protective aggregation. Prion *5*, 285–290. https://doi.org/10.4161/pri.5.4.18071.

Duennwald, M.L., Jagadish, S., Giorgini, F., Muchowski, P.J., and Lindquist, S. (2006a). A network of protein interactions determines polyglutamine toxicity. Proc. Natl. Acad. Sci. USA *103*, 11051–11056. https://doi.org/10.1073/pnas.0604548103.

Duennwald, M.L., Jagadish, S., Muchowski, P.J., and Lindquist, S. (2006b). Flanking sequences profoundly alter polyglutamine toxicity in yeast. Proc. Natl. Acad. Sci. USA *103*, 11045–11050. https://doi.org/10.1073/pnas.0604547103.

Espinosa Angarica, V.E., Angulo, A., Giner, A., Losilla, G., Ventura, S., and Sancho, J. (2014). PrionScan: an online database of predicted prion domains in complete proteomes. BMC Genomics *15*, 102. https://doi.org/10.1186/1471-2164-15-102.

Fan, C.-Y., Lee, S., Ren, H.Y., and Cyr, D.M. (2004). Exchangeable chaperone modules contribute to specification of type I and type II Hsp40 cellular function. Mol. Biol. Cell *15*, 761–773. https://doi.org/10.1091/mbc.e03-03-0146.

Fu, H., Hardy, J., and Duff, K.E. (2018). Selective vulnerability in neurodegenerative diseases. Nat. Neurosci. *21*, 1350–1358. https://doi.org/10.1038/s41593-018-0221-2.

Gandhi, J., Antonelli, A.C., Afridi, A., Vatsia, S., Joshi, G., Romanov, V., Murray, I.V.J., and Khan, S.A. (2019). Protein misfolding and aggregation in neurodegenerative diseases: a review of pathogeneses, novel detection strategies, and potential therapeutics. Rev. Neurosci. *30*, 339–358. https://doi.org/10.1515/revneuro-2016-0035.

Gene Ontology Consortium (2021). The Gene Ontology resource: enriching a GOld mine. Nucleic Acids Res. *49*, D325–D334. https://doi.org/10.1093/nar/gkaa1113.

Giasson, B.I., Forman, M.S., Higuchi, M., Golbe, L.I., Graves, C.L., Kotzbauer, P.T., Trojanowski, J.Q., and Lee, V.M. (2003). Initiation and synergistic fibrillization of Tau and alpha-synuclein. Science *300*, 636–640. https://doi.org/10.1126/science.1082324.

Gidalevitz, T., Ben-Zvi, A., Ho, K.H., Brignull, H.R., and Morimoto, R.I. (2006). Progressive disruption of cellular protein folding in models of polyglutamine diseases. Science *311*, 1471–1474. https://doi.org/10.1126/science.1124514.

Gokhale, K.C., Newnam, G.P., Sherman, M.Y., and Chernoff, Y.O. (2005). Modulation of prion-dependent polyglutamine aggregation and toxicity by chaperone proteins in the yeast model. J. Biol. Chem. *280*, 22809–22818. https://doi.org/10.1074/jbc.M500390200.

Guo, J.L., Covell, D.J., Daniels, J.P., Iba, M., Stieber, A., Zhang, B., Riddle, D.M., Kwong, L.K., Xu, Y., Trojanowski, J.Q., and Lee, V.M. (2013). Distinct alpha-synuclein strains differentially promote Tau inclusions in neurons. Cell *154*, 103–117. https://doi.org/10.1016/j.cell.2013.05.057.

Gusella, J.F., and MacDonald, M.E. (2000). Molecular genetics: unmasking polyglutamine triggers in neurodegenerative disease. Nat. Rev. Neurosci. *1*, 109–115. https://doi.org/10.1038/35039051.

Haass, C., and Selkoe, D.J. (2007). Soluble protein oligomers in neurodegeneration: lessons from the Alzheimer's amyloid β-peptide. Nat. Rev. Mol. Cell Biol. *8*, 101–112. https://doi.org/10.1038/nrm2101.

Hardenberg, M., Horvath, A., Ambrus, V., Fuxreiter, M., and Vendruscolo, M. (2020). Widespread occurrence of the droplet state of proteins in the human proteome. Proc. Natl. Acad. Sci. USA *117*, 33254–33262. https://doi.org/10.1073/pnas.2007670117.

Harding, R.J., Loppnau, P., Ackloo, S., Lemak, A., Hutchinson, A., Hunt, B., Holehouse, A.S., Ho, J.C., Fan, L., Toledo-Sherman, L., et al. (2019). Design and characterization of mutant and wildtype huntingtin proteins produced from a toolkit of scalable eukaryotic expression systems. J. Biol. Chem. *294*, 6986–7001. https://doi.org/10.1074/jbc.RA118.007204.

Harel, I., Chen, Y.R., Ziv, I., Singh, P.P., Negredo, P.N., Goshtchevsky, U., Wang, W., Astre, G., Moses, E., McKay, A., et al. (2022). Identification of protein aggregates in the aging vertebrate brain with prion-like and phase separation properties. Preprint at bioRxiv. https://doi.org/10.1101/2022.02.26.482115.

Hartl, F.U. (2017). Protein misfolding diseases. Annu. Rev. Biochem. *86*, 21–26. https://doi.org/10.1146/annurev-biochem-061516-044518.

Hazeki, N., Tukamoto, T., Goto, J., and Kanazawa, I. (2000). Formic acid dissolves aggregates of an N-terminal huntingtin fragment containing an expanded polyglutamine tract: applying to quantification of protein components of the aggregates. Biochem. Biophys. Res. Commun. *277*, 386–393. https://doi.org/10.1006/bbrc.2000.3682.

Hipp, M.S., Park, S.H., and Hartl, F.U. (2014). Proteostasis impairment in protein-misfolding and -aggregation diseases. Trends Cell Biol. *24*, 506–514. https://doi.org/10.1016/j.tcb.2014.05.003.

Hosp, F., Gutiérrez-Ángel, S., Schaefer, M.H., Cox, J., Meissner, F., Hipp, M.S., Hartl, F.U., Klein, R., Dudanova, I., and Mann, M. (2017). Spatiotemporal proteomic profiling of Huntington's disease inclusions reveals widespread loss of protein function. Cell Rep. *21*, 2291–2303. https://doi.org/10.1016/j.celrep.2017.10.097.

Iglesias, V., Paladin, L., Juan-Blanco, T., Pallarès, I., Aloy, P., Tosatto, S.C.E., and Ventura, S. (2019). In silico characterization of human prion-like proteins: beyond neurological diseases. Front. Physiol. *10*, 314. https://doi.org/10.3389/fphys.2019.00314.

Kaganovich, D., Kopito, R., and Frydman, J. (2008). Misfolded proteins partition between two distinct quality control compartments. Nature *454*, 1088–1095. https://doi.org/10.1038/nature07195.

Kato, M., Han, T.W., Xie, S., Shi, K., Du, X., Wu, L.C., Mirzaei, H., Goldsmith, E.J., Longgood, J., Pei, J., et al. (2012). Cell-free formation of RNA granules: low complexity sequence domains form dynamic fibers within hydrogels. Cell *149*, 753–767. https://doi.org/10.1016/j.cell.2012.04.017.

Kayed, R., Head, E., Thompson, J.L., McIntire, T.M., Milton, S.C., Cotman, C.W., and Glabe, C.G. (2003). Common structure of soluble amyloid oligomers implies common mechanism of pathogenesis. Science *300*, 486–489. https://doi.org/10.1126/science.1079469.

Kazantsev, A., Preisinger, E., Dranovsky, A., Goldgaber, D., and Housman, D. (1999). Insoluble detergent-resistant aggregates form between pathological and nonpathological lengths of polyglutamine in mammalian cells. Proc. Natl. Acad. Sci. USA *96*, 11404–11409. https://doi.org/10.1073/pnas.96.20.11404.

Khurana, V., and Lindquist, S. (2010). Modelling neurodegeneration in *Saccharomyces cerevisiae*: why cook with baker's yeast? Nat. Rev. Neurosci. *11*, 436–449. https://doi.org/10.1038/nrn2809.

Kim, S., Nollen, E.A., Kitagawa, K., Bindokas, V.P., and Morimoto, R.I. (2002). Polyglutamine protein aggregates are dynamic. Nat. Cell Biol. *4*, 826–831. https://doi.org/10.1038/ncb863.

Kim, Y.E., Hosp, F., Frottin, F., Ge, H., Mann, M., Hayer-Hartl, M., and Hartl, F.U. (2016). Soluble oligomers of polyQ-expanded huntingtin target a multiplicity of key cellular factors. Mol. Cell *63*, 951–964. https://doi.org/10.1016/j.molcel.2016.07.022.

Klaips, C.L., Hochstrasser, M.L., Langlois, C.R., and Serio, T.R. (2014). Spatial quality control bypasses cell-based limitations on proteostasis to promote prion curing. eLife *3*, e04288. https://doi.org/10.7554/eLife.04288.

Klaips, C.L., Jayaraj, G.G., and Hartl, F.U. (2018). Pathways of cellular proteostasis in aging and disease. J. Cell Biol. *217*, 51–63. https://doi.org/10.1083/jcb.201709072.

Klaips, C.L., Gropp, M.H.M., Hipp, M.S., and Hartl, F.U. (2020). Sis1 potentiates the stress response to protein aggregation and elevated temperature. Nat. Commun. *11*, 6271. https://doi.org/10.1038/s41467-020-20000-x.

Kremer, B., Goldberg, P., Andrew, S.E., Theilmann, J., Telenius, H., Zeisler, J., Squitieri, F., Lin, B., Bassett, A., Almqvist, E., et al. (1994). A worldwide study of the Huntingtons's disease mutation. The sensitivity and specificity of measuring CAG repeats. N. Engl. J. Med. *330*, 1401–1406. https://doi.org/10.1056/NEJM199405193302001.

Krobitsch, S., and Lindquist, S. (2000). Aggregation of huntingtin in yeast varies with the length of the polyglutamine expansion and the expression of chaperone proteins. Proc. Natl. Acad. Sci. USA *97*, 1589–1594. https://doi.org/10.1073/pnas.97.4.1589.

Kyung, T., Lee, S., Kim, J.E., Cho, T., Park, H., Jeong, Y.M., Kim, D., Shin, A., Kim, S., Baek, J., et al. (2015). Optogenetic control of endogenous Ca(2+) channels *in vivo*. Nat. Biotechnol. *33*, 1092–1096. https://doi.org/10.1038/nbt.3350.

Labbadia, J., and Morimoto, R.I. (2015). The biology of proteostasis in aging and disease. Annu. Rev. Biochem. *84*, 435–464. https://doi.org/10.1146/annurev-biochem-060614-033955.

Leitman, J., Ulrich Hartl, F., and Lederkremer, G.Z. (2013). Soluble forms of polyQ-expanded huntingtin rather than large aggregates cause endoplasmic reticulum stress. Nat. Commun. *4*, 2753. https://doi.org/10.1038/ncomms3753.

Liebman, S.W., and Chernoff, Y.O. (2012). Prions in yeast. Genetics *191*, 1041–1072. https://doi.org/10.1534/genetics.111.137760.

Liu, X.-D., Liu, P.C.C., Santoro, N., and Thiele, D.J. (1997). Conservation of a stress response: human heat shock transcription factors functionally substitute for yeast HSF. EMBO J. *16*, 6466–6477. https://doi.org/10.1093/emboj/16.21.6466.

Lopez, N., Aron, R., and Craig, E.A. (2003). Specificity of class II Hsp40 Sis1 in maintenance of yeast prion [RNQ+]. Mol. Biol. Cell *14*, 1172–1181. https://doi.org/10.1091/mbc.e02-09-0593.

Ma, L., Guan, Z., Wang, Q., Yan, X., Wang, J., Wang, Z., Cao, J., Zhang, D., Gong, X., and Yin, P. (2020). Structural insights into the photoactivation of *Arabidopsis* CRY2. Nat. Plants *6*, 1432–1438. https://doi.org/10.1038/s41477-020-00800-1.

March, Z.M., King, O.D., and Shorter, J. (2016). Prion-like domains as epigenetic regulators, scaffolds for subcellular organization, and drivers of neurodegenerative disease. Brain Res. *1647*, 9–18. https://doi.org/10.1016/j.brainres.2016.02.037.

Más, P., Devlin, P.F., Panda, S., and Kay, S.A. (2000). Functional interaction of Phytochrome B and Cryptochrome 2. Nature *408*, 207–211. https://doi.org/10.1038/35041583.

Meriin, A.B., Zhang, X., He, X., Newnam, G.P., Chernoff, Y.O., and Sherman, M.Y. (2002). Huntington toxicity in yeast model depends on polyglutamine aggregation mediated by a prion-like protein Rnq1. J. Cell Biol. *157*, 997–1004. https://doi.org/10.1083/jcb.200112104.

Mi, H., Muruganujan, A., Ebert, D., Huang, X., and Thomas, P.D. (2019). PANTHER version 14: more genomes, a new PANTHER GO-slim and improvements in enrichment analysis tools. Nucleic Acids Res. *47*, D419–D426. https://doi.org/10.1093/nar/gky1038.

Moosavi, B., Mousavi, B., and Macreadie, I.G. (2015). Yeast model of Amyloid-beta and Tau aggregation in Alzheimer's disease. J. Alzheimers Dis. *47*, 9–16. https://doi.org/10.3233/JAD-150173.

Morales, R., Moreno-Gonzalez, I., and Soto, C. (2013). Cross-seeding of misfolded proteins: implications for etiology and pathogenesis of protein misfolding diseases. PLOS Pathog. *9*. e1003537. https://doi.org/10.1371/journal.ppat.1003537.g001.

Muchowski, P.J., Schaffar, G., Sittler, A., Wanker, E.E., Hayer-Hartl, M.K., and Hartl, F.U. (2000). Hsp70 and hsp40 chaperones can inhibit self-assembly of polyglutamine proteins into amyloid-like fibrils. Proc. Natl. Acad. Sci. USA *97*, 7841–7846. https://doi.org/10.1073/pnas.140202897.

Muchowski, P.J., Ning, K., D'Souza-Schorey, C., and Fields, S. (2002). Requirement of an intact microtubule cytoskeleton for aggregation and inclusion body formation by a mutant huntingtin fragment. Proc. Natl. Acad. Sci. USA *99*, 727–732. https://doi.org/10.1073/pnas.022628699.

Mumberg, D., Müller, R., and Funk, M. (1994). Regulatable promoters of *Saccharomyces cerevisiae*: comparison of transcriptional activity and their use for heterologous expression. Nucleic Acids Res. *22*, 5767–5768. https://doi.org/10.1093/nar/22.25.5767.

Mumberg, D., Müller, R., and Funk, M. (1995). Yeast vectors for the controlled expression of heterologous proteins in different genetic backgrounds. Gene *156*, 119–122. https://doi.org/10.1016/0378-1119(95)00037-7.

Olzscha, H., Schermann, S.M., Woerner, A.C., Pinkert, S., Hecht, M.H., Tartaglia, G.G., Vendruscolo, M., Hayer-Hartl, M., Hartl, F.U., and Vabulas, R.M. (2011). Amyloid-like aggregates sequester numerous metastable proteins with essential cellular functions. Cell *144*, 67–78. https://doi.org/10.1016/j.cell.2010.11.050.

Osherovich, L.Z., and Weissman, J.S. (2001). Multiple Gln/Asn-rich prion domains confer susceptibility to induction of the yeast [PSI+] prion. Cell *106*, 183–194. https://doi.org/10.1016/S0092-8674(01)00440-8.

Osherovich, L.Z., and Weissman, J.S. (2002). The utility of prions. Dev. Cell *2*, 143–151. https://doi.org/10.1016/s1534-5807(02)00118-1.

Ossato, G., Digman, M.A., Aiken, C., Lukacsovich, T., Marsh, J.L., and Gratton, E. (2010). A two-step path to inclusion formation of huntingtin peptides revealed by number and brightness analysis. Biophys. J. *98*, 3078–3085. https://doi.org/10.1016/j.bpj.2010.02.058.

Palayam, M., Ganapathy, J., Guercio, A.M., Tal, L., Deck, S.L., and Shabek, N. (2021). Structural insights into photoactivation of plant Cryptochrome-2. Commun. Biol. *4*, 28. https://doi.org/10.1038/s42003-020-01531-x.

Park, S.H., Kukushkin, Y., Gupta, R., Chen, T., Konagai, A., Hipp, M.S., Hayer-Hartl, M., and Hartl, F.U. (2013). PolyQ proteins interfere with nuclear degradation of cytosolic proteins by sequestering the Sis1p chaperone. Cell *154*, 134–145. https://doi.org/10.1016/j.cell.2013.06.003.

Pathak, G.P., Spiltoir, J.I., Höglund, C., Polstein, L.R., Heine-Koskinen, S., Gersbach, C.A., Rossi, J., and Tucker, C.L. (2017). Bidirectional approaches for optogenetic regulation of gene expression in mammalian cells using *Arabidopsis* Cryptochrome 2. Nucleic Acids Res. *45*, e167. https://doi.org/10.1093/nar/gkx260.

Peskett, T.R., Rau, F., O'Driscoll, J., Patani, R., Lowe, A.R., and Saibil, H.R. (2018). A liquid to solid phase transition underlying pathological huntingtin exon1 aggregation. Mol. Cell *70*, 588–601.e6. https://doi.org/10.1016/j.molcel.2018.04.007.

Rappsilber, J., Mann, M., and Ishihama, Y. (2007). Protocol for micro-purification, enrichment, pre-fractionation and storage of peptides for proteomics using StageTips. Nat. Protoc. *2*, 1896–1906. https://doi.org/10.1038/nprot.2007.261.

Ripaud, L., Chumakova, V., Antonin, M., Hastie, A.R., Pinkert, S., Körner, R., Ruff, K.M., Pappu, R.V., Hornburg, D., Mann, M., et al. (2014). Overexpression of Q-rich prion-like proteins suppresses polyQ cytotoxicity and alters the polyQ interactome. Proc. Natl. Acad. Sci. USA *111*, 18219–18224. https://doi.org/10.1073/pnas.1421313111.

Ross, C.A., and Poirier, M.A. (2004). Protein aggregation and neurodegenerative disease. Nat. Med. *10*, S10–S17. https://doi.org/10.1038/nm1066.

Rupp, S. (2002). LacZ assays in yeast. Methods Enzymol. *350*, 112–131. https://doi.org/10.1016/S0076-6879(02)50959-9.

Schaffar, G., Breuer, P., Boteva, R., Behrends, C., Tzvetkov, N., Strippel, N., Sakahira, H., Siegers, K., Hayer-Hartl, M., and Hartl, F.U. (2004). Cellular toxicity of polyglutamine expansion proteins: mechanism of transcription factor deactivation. Mol. Cell *15*, 95–105. https://doi.org/10.1016/j.molcel.2004.06.029.

Scherzinger, E., Lurz, R., Turmaine, M., Mangiarini, L., Hollenbach, B., Hasenbank, R., Bates, G.P., Davies, S.W., Lehrach, H., and Wanker, E.E. (1997). Huntingtin-encoded polyglutamine expansions form amyloid-like protein aggregates *in vitro* and *in vivo*. Cell *90*, 549–558. https://doi.org/10.1016/S0092-8674(00)80514-0.

Schindelin, J., Arganda-Carreras, I., Frise, E., Kaynig, V., Longair, M., Pietzsch, T., Preibisch, S., Rueden, C., Saalfeld, S., Schmid, B., et al. (2012). Fiji: an open-source platform for biological-image analysis. Nat. Methods *9*, 676–682. https://doi.org/10.1038/nmeth.2019.

Schwanhäusser, B., Busse, D., Li, N., Dittmar, G., Schuchhardt, J., Wolf, J., Chen, W., and Selbach, M. (2011). Global quantification of mammalian gene expression control. Nature *473*, 337–342. https://doi.org/10.1038/nature10098.

Serio, T.R. (2018). [PIN+]ing down the mechanism of prion appearance. FEMS Yeast Res. *18*, foy026. https://doi.org/10.1093/femsyr/foy026.

Sharma, K., Schmitt, S., Bergner, C.G., Tyanova, S., Kannaiyan, N., Manrique-Hoyos, N., Kongi, K., Cantuti, L., Hanisch, U.K., Philips, M.A., et al. (2015). Cell type- and brain region-resolved mouse brain proteome. Nat. Neurosci. *18*, 1819–1831. https://doi.org/10.1038/nn.4160.

Shin, Y., Berry, J., Pannucci, N., Haataja, M.P., Toettcher, J.E., and Brangwynne, C.P. (2017). Spatiotemporal control of intracellular phase transitions using light-activated optoDroplets. Cell *168*, 159–171.e14. https://doi.org/10.1016/j.cell.2016.11.054.

Sikorski, R.S., and Hieter, P. (1989). A system of shuttle vectors and yeast host strains designed for efficient manipulation of DNA in *Saccharomyces cerevisiae*. Genetics *122*, 19–27. https://doi.org/10.1093/genetics/122.1.19.

Sinnige, T., Meisl, G., Michaels, T.C.T., Vendruscolo, M., Knowles, T.P.J., and Morimoto, R.I. (2021). Kinetic analysis reveals that independent nucleation events determine the progression of polyglutamine aggregation in C. elegans. Proc. Natl. Acad. Sci. USA *118*. e2021888118. https://doi.org/10.1073/pnas.2021888118.

Sondheimer, N., and Lindquist, S. (2000). Rnq1: an epigenetic modifier of protein function in yeast. Mol. Cell *5*, 163–172. https://doi.org/10.1016/s1097-2765(00)80412-8.

Sondheimer, N., Lopez, N., Craig, E.A., and Lindquist, S. (2001). The role of Sis1 in the maintenance of the [RNQ+] prion. EMBO J. *20*, 2435–2442. https://doi.org/10.1093/emboj/20.10.2435.

Sprunger, M.L., and Jackrel, M.E. (2021). Prion-like proteins in phase separation and their link to disease. Biomolecules *11*, 1014. https://doi.org/10.3390/biom11071014.

Stefani, M., and Dobson, C.M. (2003). Protein aggregation and aggregate toxicity: new insights into protein folding, misfolding diseases and biological evolution. J. Mol. Med. (Berl) *81*, 678–699. https://doi.org/10.1007/s00109-003-0464-5.

Takahashi, T., Kikuchi, S., Katada, S., Nagai, Y., Nishizawa, M., and Onodera, O. (2008). Soluble polyglutamine oligomers formed prior to inclusion body formation are cytotoxic. Hum. Mol. Genet. *17*, 345–356. https://doi.org/10.1093/hmg/ddm311.

Taslimi, A., Vrana, J.D., Chen, D., Borinskaya, S., Mayer, B.J., Kennedy, M.J., and Tucker, C.L. (2014). An optimized optogenetic clustering tool for probing protein interaction and function. Nat. Commun. *5*, 4925. https://doi.org/10.1038/ncomms5925.

Tuite, M.F., Mundy, C.R., and Cox, B.S. (1981). Agents that cause a high frequency of genetic change from [PSI+] to [psi−] in *Saccharomyces cerevisiae*. Genetics *98*, 691–711. https://doi.org/10.1093/genetics/98.4.691.

Tyanova, S., Temu, T., Sinitcyn, P., Carlson, A., Hein, M.Y., Geiger, T., Mann, M., and Cox, J. (2016). The Perseus computational platform for

comprehensive analysis of (prote)omics data. Nat. Methods *13*, 731–740. https://doi.org/10.1038/nmeth.3901.

Vasconcelos, B., Stancu, I.C., Buist, A., Bird, M., Wang, P., Vanoosthuyse, A., Van Kolen, K., Verheyen, A., Kienlen-Campard, P., Octave, J.N., et al. (2016). Heterotypic seeding of Tau fibrillization by pre-aggregated Abeta provides potent seeds for prion-like seeding and propagation of Tau-pathology *in vivo*. Acta Neuropathol. *131*, 549–569. https://doi.org/10.1007/s00401-015-1525-x.

Vecchi, G., Sormanni, P., Mannini, B., Vandelli, A., Tartaglia, G.G., Dobson, C.M., Hartl, F.U., and Vendruscolo, M. (2020). Proteome-wide observation of the phenomenon of life on the edge of solubility. Proc. Natl. Acad. Sci. USA *117*, 1015–1020. https://doi.org/10.1073/pnas.1910444117.

Verghese, J., Abrams, J., Wang, Y., and Morano, K.A. (2012). Biology of the heat shock response and protein chaperones: budding yeast (*Saccharomyces cerevisiae*) as a model system. Microbiol. Mol. Biol. Rev. *76*, 115–158. https://doi.org/10.1128/MMBR.05018-11.

Vitalis, A., and Pappu, R.V. (2011). Assessing the contribution of heterogeneous distributions of oligomers to aggregation mechanisms of polyglutamine peptides. Biophys. Chem. *159*, 14–23. https://doi.org/10.1016/j.bpc.2011.04.006.

Vitrenko, Y.A., Gracheva, E.O., Richmond, J.E., and Liebman, S.W. (2007). Visualization of aggregation of the Rnq1 prion domain and cross-seeding interactions with Sup35NM. J. Biol. Chem. *282*, 1779–1787. https://doi.org/10.1074/jbc.M609269200.

Wach, A., Brachat, A., Pöhlmann, R., and Philippsen, P. (1994). New heterologous modules for classical or PCR-based gene disruptions in *Saccharomyces cerevisiae*. Yeast *10*, 1793–1808. https://doi.org/10.1002/yea.320101310.

Walker, F.O. (2007). Huntington's disease. Lancet *369*, 218–228. https://doi.org/10.1016/s0140-6736(07)60111-1.

Walters, R.H., and Murphy, R.M. (2011). Aggregation kinetics of interrupted polyglutamine peptides. J. Mol. Biol. *412*, 505–519. https://doi.org/10.1016/j.jmb.2011.07.003.

Walther, D.M., Kasturi, P., Zheng, M., Pinkert, S., Vecchi, G., Ciryam, P., Morimoto, R.I., Dobson, C.M., Vendruscolo, M., Mann, M., and Hartl, F.U. (2015). Widespread proteome remodeling and aggregation in aging *C. elegans*. Cell *161*, 919–932. https://doi.org/10.1016/j.cell.2015.03.032.

Wang, Q., and Lin, C. (2020). Mechanisms of cryptochrome-mediated photoresponses in plants. Annu. Rev. Plant Biol. *71*, 103–129. https://doi.org/10.1146/annurev-arplant-050718-100300.

Wang, Y., Meriin, A.B., Zaarur, N., Romanova, N.V., Chernoff, Y.O., Costello, C.E., and Sherman, M.Y. (2009). Abnormal proteins can form aggresome in yeast: aggresome-targeting signals and components of the machinery. FASEB J. *23*, 451–463. https://doi.org/10.1096/fj.08-117614.

Wetzel, R. (2012). Physical chemistry of polyglutamine: intriguing tales of a monotonous sequence. J. Mol. Biol. *421*, 466–490. https://doi.org/10.1016/j.jmb.2012.01.030.

Wickner, R.B. (2016). Yeast and fungal prions. Cold Spring Harb. Perspect. Biol. *8*, a023531. https://doi.org/10.1101/cshperspect.a023531.

Wickner, R.B., Edskes, H.K., Roberts, B.T., Pierce, M.M., Baxa, U., and Ross, E. (2001). Prions beget prions: the [PIN+] mystery! Trends Biochem. Sci. *26*, 697–699. https://doi.org/10.1016/s0968-0004(01)02020-5.

Winderickx, J., Delay, C., De Vos, A., Klinger, H., Pellens, K., Vanhelmont, T., Van Leuven, F., and Zabrocki, P. (2008). Protein folding diseases and neurodegeneration: lessons learned from yeast. Biochim. Biophys. Acta *1783*, 1381–1395. https://doi.org/10.1016/j.bbamcr.2008.01.020.

Wootton, J.C., and Federhen, S. (1993). Statistics of local complexity in amino acid sequences and sequence databases. Comput. Chem. *17*, 149–163. https://doi.org/10.1016/0097-8485(93)85006-X.

Yushchenko, T., Deuerling, E., and Hauser, K. (2018). Insights into the aggregation mechanism of polyQ proteins with different glutamine repeat lengths. Biophys. J. *114*, 1847–1857. https://doi.org/10.1016/j.bpj.2018.02.037.

Zbinden, A., Pérez-Berlanga, M., De Rossi, P., and Polymenidou, M. (2020). Phase separation and neurodegenerative diseases: a disturbance in the force. Dev. Cell *55*, 45–68. https://doi.org/10.1016/j.devcel.2020.09.014.

STAR★METHODS

KEY RESOURCES TABLE

REAGENT or RESOURCE	SOURCE	IDENTIFIER
Antibodies		
mCherry Monoclonal Antibody (16D7)	Invitrogen	Cat#M11217; RRID:AB_2536611
PGK1 Monoclonal Antibody (22C5D8)	Invitrogen	Cat#459250; RRID:AB_2532235
Anti Sis1(Dnaj) pAb (Rabbit)	Cosmo Bio USA	Cat#COP-080051; RRID:AB_10709957
Monoclonal Anti-c-Myc antibody produced in mouse	Sigma	Cat#M5546; RRID:AB_260581
Anti-Rat IgG (whole molecule)-Peroxidase antibody produced in goat	Sigma	Cat#A9037; RRID:AB_258429
Anti-Mouse IgG (whole molecule)-Peroxidase antibody produced in goat	Sigma	Cat#A4416; RRID:AB_258167
Anti-Rabbit IgG (whole molecule)–Peroxidase antibody produced in goat	Sigma	Cat#A9169; RRID:AB_258434
Bacterial and virus strains		
Escherichia coli Bl21(DE3)	Sigma	Cat#69450
Escherichia coli DH5α	Invitrogen	Cat#18265017
Chemicals, peptides, and recombinant proteins		
2-Nitrophenyl β-D-galactopyranoside (ONPG)	Sigma	Cat#N1127
AatII restriction enzyme	New England BioLabs	Cat#R0117
AflII restriction enzyme	New England BioLabs	Cat#R0520
BglII restriction enzyme	New England BioLabs	Cat#R0144
BsgI restriction enzyme	New England BioLabs	Cat#R0559
Bsu36I restriction enzyme	New England BioLabs	Cat#R0524
cOmplete, EDTA-free Protease Inhibitor Cocktail	Roche	Cat#COEDTAF-RO
Concanavalin A from *Canavalia ensiformis*	Sigma	Cat#C2010
Cycloheximide	Sigma	Cat#01810
Doxycycline	Sigma	Cat#D3072
DraIII restriction enzyme	New England BioLabs	Cat#R3510
EcoRI restriction enzyme	New England BioLabs	Cat#R3101
Geneticin Selective Antibiotic (G418 Sulfate)	Gibco	Cat#10131027
Gibson Assembly Master Mix	New England BioLabs	Cat#2611
GST-PreScission Protease	MPI Biochemistry	N/A
Guanidine-HCl Solution (8M)	Thermo Scientific	Cat#24115
Isopropyl β-D-1-thiogalactopyranoside (IPTG)	Roth	Cat#CN08.3
KpnI restriction enzyme	New England BioLabs	Cat#R3142
NdeI restriction enzyme	New England BioLabs	Cat#R0111
n-Octyl-β-D-glucopyranoside (OGP)	Roth	Cat#CN23.1
PvuI restriction enzyme	New England BioLabs	Cat#R0150
Q5 High-fidelity DNA Polymerase	New England BioLabs	Cat#0491
SacI restriction enzyme	New England BioLabs	Cat#R3156
SalI restriction enzyme	New England BioLabs	Cat#R3138
Serratia marcescens DNase	MPI Biochemistry	N/A
SpeI restriction enzyme	New England BioLabs	Cat#R3133
StuI restriction enzyme	New England BioLabs	Cat#R0187
T7 DNA Ligase	New England BioLabs	Cat#0318
Trypsin recombinant, Proteomics Grade	Roche	Cat#RTRYP-RO

(*Continued on next page*)

Continued

REAGENT or RESOURCE	SOURCE	IDENTIFIER
Trypsin recombinant, Sequence Grad	Promega	Cat#V5111
XbaI restriction enzyme	New England BioLabs	Cat#R0145
XhoI restriction enzyme	New England BioLabs	Cat#R0146
Critical commercial assays		
Bio-Rad Protein Assay Kit	Bio-Rad Laboratories	Cat#5000001
Immobilon Classico Western HRP Substrate	Millipore	Cat#WBLUC0500
Pierce Rapid Gold BCA Protein Assay Kit	Thermo Scientific	Cat#A53227
Deposited data		
Proteomic dataset	This study	Tables S2, S3, and S4; ProteomeXchange: PXD031337
Proteomic dataset (related to discussion)	Kim et al. (2016)	ProteomeXchange: PXD003446
Proteomic dataset (related to discussion)	Sharma et al. (2015)	ProteomeXchange: PXD001250
Experimental models: Organisms/strains		
74-D694 MATa [*PIN*$^+$] ade1-14 his3-11,-15 trp1-1 ura3-1 leu2-3, 112 can1-100	SY197 in Klaips et al. (2014)	N/A
74-D694 MATa [*PIN*$^+$] ade1-14 his3-11,-15 trp1-1 ura3-1 leu2-3,112 can1-100 pdr5Δ::kanMX	This study	yMG33
74-D694 MATa [*PIN*$^+$] ade1-14 his3-11,-15 trp1-1 ura3-1 can1-100 pdr5Δ::kanMX leu2-3,112::LEU::P_{GPD}mCherry-Cry2olig	This study	yMG49 (yMG33+pMG60)
74-D694 MATa [*PIN*$^+$] ade1-14 his3-11,-15 trp1-1 ura3-1 can1-100 pdr5Δ::kanMX leu2-3,112::LEU::P_{GPD}Htt97Q-mCherry-Cry2olig	This study	yMG78 (yMG33+pMG148)
74-D694 MATa [*PIN*$^+$] ade1-14 his3-11,-15 trp1-1 ura3-1 can1-100 pdr5Δ::kanMX leu2-3,112::LEU::P_{GPD}Htt20Q-mCherry-Cry2olig	This study	yMG88 (yMG33+pMG154)
74-D694 MATa [*pin*$^-$] ade1-14 his3-11,-15 trp1-1 ura3-1 can1-100 pdr5Δ::kanMX leu2-3,112::LEU::P_{GPD}mCherry-Cry2olig	This study	yMG91 (yMG49 cured)
74-D694 MATa [*pin*$^-$] ade1-14 his3-11,-15 trp1-1 ura3-1 can1-100 pdr5Δ::kanMX leu2-3,112::LEU::P_{GPD}Htt97Q-mCherry-Cry2olig	This study	yMG92 (yMG78 cured)
74-D694 MATa [*pin*$^-$] ade1-14 his3-11,-15 trp1-1 ura3-1 can1-100 pdr5Δ::kanMX leu2-3,112::LEU::P_{GPD}Htt20Q-mCherry-Cry2olig	This study	yMG94 (yMG88 cured)
74-D694 MATa [*pin*$^-$] ade1-14 his3-11,-15 ura3-1 can1-100 pdr5Δ::kanMX leu2-3,112::LEU::P_{GPD}mCherry-Cry2olig trp11::TRP::P_{GPD}Htt97Q-GFP	This study	yMG103 (yMG91+pMG160)
74-D694 MATa [*pin*$^-$] ade1-14 his3-11,-15 ura3-1 can1-100 pdr5Δ::kanMX leu2-3,112::LEU::P_{GPD}Htt97Q-mCherry-Cry2olig trp11::TRP::P_{GPD}Htt97Q-GFP	This study	yMG104 (yMG92+pMG160)
74-D694 MATa [*pin*$^-$] ade1-14 his3-11,-15 ura3-1 can1-100 pdr5Δ::kanMX leu2-3,112::LEU::P_{GPD}Htt20Q-mCherry-Cry2olig trp11::TRP::P_{GPD}Htt20Q-GFP	This study	yMG106 (yMG94+pMG161)
74-D694 MATa [*pin*$^-$] ade1-14 his3-11,-15 ura3-1 can1-100 pdr5Δ::kanMX leu2-3,112::LEU::P_{GPD}mCherry-Cry2olig trp11::TRP::P_{GPD}Htt20Q-GFP	This study	yMG120 (yMG91+pMG161)
74-D694 MATa [*pin*$^-$] ade1-14 his3-11,-15 ura3-1 can1-100 pdr5Δ::kanMX leu2-3,112::LEU::P_{GPD}Htt97Q-mCherry-Cry2olig trp11::TRP::P_{GPD}Htt20Q-GFP	This study	yMG121 (yMG92+pMG161)
74-D694 MATa [*pin*$^-$] ade1-14 his3-11,-15 ura3-1 can1-100 pdr5Δ::kanMX leu2-3,112::LEU::P_{GPD}Htt20Q-mCherry-Cry2olig trp11::TRP::P_{GPD}Htt97Q-GFP	This study	yMG122 (yMG94+pMG160)
74-D694 MATa [*PIN*$^+$] ade1-14 his3-11,-15 trp1-1 ura3-1 can1-100 pdr5Δ::kanMX leu2-3,112::LEU::P_{GPD}Htt36Q-mCherry-Cry2olig	This study	yMG186 (yMG33+pMG190)
74-D694 MATa [*PIN*$^+$] ade1-14 his3-11,-15 trp1-1 ura3-1 can1-100 pdr5Δ::kanMX leu2-3,112::LEU::P_{GPD}Htt48Q-mCherry-Cry2olig	This study	yMG187 (yMG33+pMG191)

(*Continued on next page*)

Continued

REAGENT or RESOURCE	SOURCE	IDENTIFIER
74-D694 MATa [*PIN*$^+$] ade1-14 his3-11,-15 trp1-1 ura3-1 can1-100 pdr5Δ::kanMX leu2-3,112::LEU::P_{GPD}Htt60Q-mCherry-Cry2olig	This study	yMG189 (yMG33+pMG193)
74-D694 MATa [*PIN*$^+$] ade1-14 his3-11,-15 trp1-1 ura3-1 can1-100 pdr5Δ::kanMX leu2-3,112::LEU::P_{GPD}Htt73Q-mCherry-Cry2olig	This study	yMG190 (yMG33+pMG194)
74-D694 MATa [*pin*$^-$] ade1-14 his3-11,-15 trp1-1 ura3-1 can1-100 pdr5Δ::kanMX leu2-3,112::LEU::P_{GPD}Htt36Q-mCherry-Cry2olig	This study	yMG198 (yMG186 cured)
74-D694 MATa [*pin*$^-$] ade1-14 his3-11,-15 trp1-1 ura3-1 can1-100 pdr5Δ::kanMX leu2-3,112::LEU::P_{GPD}Htt48Q-mCherry-Cry2olig	This study	yMG199 (yMG187 cured)
74-D694 MATa [*pin*$^-$] ade1-14 his3-11,-15 trp1-1 ura3-1 can1-100 pdr5Δ::kanMX leu2-3,112::LEU::P_{GPD}Htt60Q-mCherry-Cry2olig	This study	yMG201 (yMG189 cured)
74-D694 MATa [*pin*$^-$] ade1-14 his3-11,-15 trp1-1 ura3-1 can1-100 pdr5Δ::kanMX leu2-3,112::LEU::P_{GPD}Htt73Q-mCherry-Cry2olig	This study	yMG202 (yMG190 cured)
YPH499 MATa [*pin*$^-$] ura3-52 lys2-801 ade2-101 trp1-Δ63 his3-Δ200 leu2-Δ1	This study	yMG206 (yMG207 cured)
YPH499 MATa [*PIN*$^+$] ura3-52 lys2-801 ade2-101 trp1-Δ63 his3-Δ200 leu2-Δ1	Sikorski and Hieter (1989)	yMG207
74-D694 MATa [*PIN*$^+$] ade1-14 his3-11,-15 trp1-1 leu2-3,112 can1-100 pdr5Δ::kanMX ura3-1::URA::P_{ADH}RNQ1-GFP	This study	yMG258 (yMG33+pMG269)
74-D694 MATa [*PIN*$^+$] ade1-14 his3-11,-15 trp1-1 can1-100 pdr5Δ::kanMX leu2-3,112::LEU::P_{GPD}mCherry-Cry2olig ura3-1::URA::P_{ADH}RNQ1-GFP	This study	yMG259 (yMG49+pMG269)
74-D694 MATa [*PIN*$^+$] ade1-14 his3-11,-15 trp1-1 can1-100 pdr5Δ::kanMX leu2-3,112::LEU::P_{GPD}Htt97Q-mCherry-Cry2olig ura3-1::URA::P_{ADH}RNQ1-GFP	This study	yMG260 (yMG78+pMG269)
74-D694 MATa [*PIN*$^+$] ade1-14 his3-11,-15 trp1-1 can1-100 pdr5Δ::kanMX leu2-3,112::LEU::P_{GPD}Htt20Q-mCherry-Cry2olig ura3-1::URA::P_{ADH}RNQ1-GFP	This study	yMG262 (yMG88+pMG269)
74-D694 MATa [*pin*$^-$] ade1-14 his3-11,-15 trp1-1 leu2-3,112 can1-100 pdr5Δ::kanMX ura3-1::URA::P_{ADH}RNQ1-GFP	This study	yMG265 (yMG258 cured)
74-D694 MATa [*pin*$^-$] ade1-14 his3-11,-15 trp1-1 can1-100 pdr5Δ::kanMX leu2-3,112::LEU::P_{GPD}mCherry-Cry2olig ura3-1::URA::P_{ADH}RNQ1-GFP	This study	yMG266 (yMG259 cured)
74-D694 MATa [*pin*$^-$] ade1-14 his3-11,-15 trp1-1 can1-100 pdr5Δ::kanMX leu2-3,112::LEU::P_{GPD}Htt97Q-mCherry-Cry2olig ura3-1::URA::P_{ADH}RNQ1-GFP	This study	yMG267 (yMG260 cured)
74-D694 MATa [*pin*$^-$] ade1-14 his3-11,-15 trp1-1 can1-100 pdr5Δ::kanMX leu2-3,112::LEU::P_{GPD}Htt20Q-mCherry-Cry2olig ura3-1::URA::P_{ADH}RNQ1-GFP	This study	yMG269 (yMG262 cured)
YPH499 MATa [*PIN*$^+$] ura3-52 lys2-801 ade2-101 trp1-Δ63::TRP:: his3-Δ200 leu2-Δ1 sis1Δ::kanMX P_{TETR}SIS1	Klaips et al. (2020)	yMG276
YPH499 MATa [*pin*$^-$] ura3-52 lys2-801 ade2-101 trp1-Δ63::TRP:: his3-Δ200 leu2-Δ1 sis1Δ::kanMX P_{TETR}SIS1	This study	yMG277 (yMG276 cured)
Oligonucleotides		
See Table S1	See Table S1	See Table S1
Recombinant DNA		
pBacMam2-DiEx-LIC-C-flag_huntingtin_full-length_Q36	Harding et al. (2019)	Addgene Cat#111745
pBacMam2-DiEx-LIC-C-flag_huntingtin_full-length_Q48	Harding et al. (2019)	Addgene Cat#111747
pBacMam2-DiEx-LIC-C-flag_huntingtin_full-length_Q54	Harding et al. (2019)	Addgene Cat#111727
pBacMam2-DiEx-LIC-C-flag_huntingtin_full-length_Q60	Harding et al. (2019)	Addgene Cat#111749
pBacMam2-DiEx-LIC-C-flag_huntingtin_full-length_Q73	Harding et al. (2019)	Addgene Cat#111728
pESC-URA-Rnq1-GFP	Kaganovich et al. (2008)	Addgene Cat#21051
pFA6aGFP(S65T)kanMX6	Bahler et al. (1998)	Addgene Cat#39292

(*Continued on next page*)

Continued

REAGENT or RESOURCE	SOURCE	IDENTIFIER
pFA6-kanMX4	Wach et al. (1994)	N/A
pGAL-CG*	Park et al. (2013)	N/A
pGEX-Htt53Q	Schaffar et al. (2004)	N/A
pHR-mCh-Cry2olig	Shin et al. (2017)	Kind gift of C. Brangwynne; Addgene Cat#101222
pRS304	Sikorski and Hieter (1989)	N/A
pRS305	Sikorski and Hieter (1989)	N/A
pRS314	Sikorski and Hieter (1989)	N/A
pRS316	Sikorski and Hieter (1989)	N/A
pRS426	Christianson et al. (1992)	N/A
pRS416pGAL	Mumberg et al. (1994)	N/A
pRS416pGPD	Mumberg et al. (1995)	N/A
pRS306pADH	Mumberg et al. (1995)	N/A
pRS414pGPD-Sis1	Douglas et al. (2008)	Addgene Cat#18687
pYES2-Htt25Q-GFP	Ripaud et al. (2014)	N/A
pYES2-Htt97Q-GFP	Ripaud et al. (2014)	N/A
pYES2-myc-20QmCh	Park et al. (2013)	N/A
pYES2-myc-97QmCh	Park et al. (2013)	N/A
Ssa3-LacZ-Leu	Liu et al. (1997)	N/A
pRS316pGPD	This study	pMG6
pRS316pGAL	This study	pMG7
pRS316pGPD_mCherry-Cry2olig	This study	pMG18
pRS305pGPD_mCherry-Cry2olig	This study	pMG60
pRS316pGAL_mCherry-Cry2olig	This study	pMG88
pRS305pGAL_mCherry-Cry2olig	This study	pMG90
pRS305pGPD _97Q-mCherry-Cry2olig	This study	pMG148
pRS305pGPD _97Q-mCherry	This study	pMG150
pRS305pGPD _20Q-mCherry-Cry2olig	This study	pMG154
pRS305pGPD _20Q-mCherry	This study	pMG155
pRS305pGPD _97Q-GFP	This study	pMG158
pRS305pGPD _20Q-GFP	This study	pMG159
pRS304pGPD _97Q-GFP	This study	pMG160
pRS304pGPD _20Q-GFP	This study	pMG161
pRS305pGPD _36Q-mCherry	This study	pMG185
pRS305pGPD _48Q-mCherry	This study	pMG186
pRS305pGPD _54Q-mCherry	This study	pMG187
pRS305pGPD _60Q-mCherry	This study	pMG188
pRS305pGPD _73Q-mCherry	This study	pMG189
pRS305pGPD _36Q-mCherry-Cry2olig	This study	pMG190
pRS305pGPD _48Q-mCherry-Cry2olig	This study	pMG191
pRS305pGPD _60Q-mCherry-Cry2olig	This study	pMG193
pRS305pGPD _73Q-mCherry-Cry2olig	This study	pMG194
pGEX-Htt20Q	This study	pMG202
pGEX-Htt54Q	This study	pMG205
pRS426pGAL_66QΔP-mCherry-Cry2olig	This study	pMG210
pRS426pGAL_mCherry-Cry2olig	This study	pMG245
pRS426pGAL_20Q-mCherry-Cry2olig	This study	pMG246
pRS426pGAL_36Q-mCherry-Cry2olig	This study	pMG247
pRS426pGAL_48Q-mCherry-Cry2olig	This study	pMG248

(*Continued on next page*)

Continued

REAGENT or RESOURCE	SOURCE	IDENTIFIER
pRS426pGAL_60Q-mCherry-Cry2olig	This study	pMG250
pRS426pGAL_73Q-mCherry-Cry2olig	This study	pMG251
pRS426pGAL_97Q-mCherry-Cry2olig	This study	pMG252
pRS426pGAL_25QΔP-mCherry-Cry2olig	This study	pMG267
pRS426pGAL_97QΔP-mCherry-Cry2olig	This study	pMG268
pRS306pADH-Rnq1GFP	This study	pMG269
pESC-URA-Rnq1-GFP_noMYC	This study	pMG271
Software and algorithms		
Fiji-ImageJ Image processing package v1.52p	Schindelin et al. (2012)	https://imagej.net/software/fiji/
GO Enrichment Analysis	Ashburner et al. (2000), Gene Ontology (2021), Mi et al. (2019)	http://geneontology.org/
GraphPad Prism v9.3.1	GraphPad Software	https://www.graphpad.com/scientific-software/prism/
MaxQuant v1.6.17.0	Cox and Mann (2008)	https://maxquant.net/maxquant/
Perseus v1.6.12.0	Tyanova et a. (2016)	https://maxquant.net/perseus/
Other		
μMACS c-myc Isolation Kit	Miltenyi Biotec	Cat#130-091-123
μMACS Columns	Miltenyi Biotec	Cat#130-042-701
μMACS GFP Isolation Kit	Miltenyi Biotec	Cat#130-091-125
μ-Slide VI-Flat Imaging Chambers	Ibidi	Cat#80621
Amersham ImageQuant 800 Western Blot Imaging System	Cytiva Life Sciences	Cat#29399481
Amersham Protran Western Blotting Membranes, nitrocellulose	Merck	Cat#GE10600002
Attune NxT Flow Cytometer	Thermo Scientific	N/A
Bioruptor Plus sonication device	Diagenode	Cat#B01020001
Cellulose acetate Membrane - OE66	Cytiva Life Sciences	Cat#10404131
EmulsiFlex-C5 High Pressure Homogenizer	Avestin	N/A
FastPrep-24 Classic Bead Beating Grinder and Lysis System	MP Biomedicals	Cat#116004500
GFP-Trap Agarose	ChromoTek	Cat#gta
GSTPrep Fast Flow 16/10	Cytiva Life Sciences	Cat#GE28-9365-50
HiPrep 26/60 Sephacryl S-100 HR	Cytiva Life Sciences	Cat#GE17-1194-01
LED Dash 1,23 m LED Tube 18 Watt 1800 Lumens Blue	Orgon	ASIN#B071GNZ5YW
NanoDrop One/OneC Microvolume UV-Vis Spectrophotometer	Thermo Scientific	Cat#ND-ONE-W
NuPAGE 4-12% Bis-Tris Gels, 1mm, 10 wells	Invitrogen	Cat#NP0321BOX
NuPAGE 4-12% Bis-Tris Gels, 1mm, 12 wells	Invitrogen	Cat#NP0322BOX
NuPAGE 4-12% Bis-Tris Gels, 1mm, 15 wells	Invitrogen	Cat#NP0323BOX
NuPAGE MOPS SDS Running Buffer (20X)	Invitrogen	Cat#NP0001
Olympus FV1000 Confocal Microscope	Olympus Life Sciences	N/A
PR648 Slot Blot Blotting Manifold	Hoefer	Cat#12004787
Q Exactive HF-X Hybrid Quadrupole-Orbitrap Mass Spectrometer	Thermo Scientific	N/A
ReproSil-Pur C18-AQ 1.9-micron beads	Dr. Maisch	Cat#r119.aq.
Restore Western Blot Stripping Buffer	Thermo Scientific	Cat#21059
Thermo Easy-nLC 1200	Thermo Scientific	Cat#LC140
Type 45 Ti Fixed-Angle Titanium Rotor	Beckman Coulter	Cat#339160
Vivaspin 6, 30 kDa MWCO	Cytiva Life Sciences	Cat#GE28-9323-17
Zeiss Plan-Apochromat 63x/1,4 Oil DIC M27	Carl Zeiss	Cat#420782-9900-799

RESOURCE AVAILABILITY

Lead contact

Further information and requests for resources and reagents should be directed to and will be fulfilled by the lead contact, F. Ulrich Hartl (uhartl@biochem.mpg.de).

Materials availability

Plasmids and yeast strains generated in this study are available upon request to the lead contact.

Data and code availability

- Mass spectrometry data have been deposited at ProteomeXchange and are publicly available as of the date of publication. The accession number is listed in the key resources table. This paper also analyzes existing, publicly available data. The accession numbers for these datasets are listed in the key resources table as well.
- This paper does not report original code.
- Any additional information required to reanalyze the data reported in this paper is available from the lead contact upon request.

EXPERIMENTAL MODEL AND SUBJECT DETAILS

All yeast strains used in this study are *Saccharomyces cerevisiae* derivatives of 74-D694 (Chernoff et al., 1995) and YPH499 (Sikorski and Hieter, 1989) and are listed in the key resources table. Cells were cultured in YPD or in synthetic complete (SC) medium at 30 °C, unless noted otherwise. Media contained either 2% glucose (YPD, SC), 2% raffinose (SCRaf) or 3% galactose and 1% raffinose (SCRaf/Gal) as carbon source depending on experimental requirements. For cultures of yeast strains carrying additional expression plasmids, nutrients necessary for plasmid selection were omitted in SC. Cells were grown in a dark room in the absence of blue light (dark or red light as light source), unless stated otherwise. For light-activation, cells were cultured with direct blue light illumination (LED Dash 1.23 m LED Tube 18 Watt 1800 Lumens Blue, Orgon) for the indicated amounts of time. Generally, cultures were maintained for >18 hours and harvested during log phase growth for analysis.

METHOD DETAILS

Molecular cloning

Recombinant DNA constructs and oligonucleotides used in this study are listed in the key resources table and Table S1. Conventional DNA cloning was performed using restriction digest and DNA ligation using T4 DNA ligase (New England Biolabs). PCR was performed using Q5 DNA polymerase (New England Biolabs). Gibson Assembly cloning was performed using Gibson Assembly Cloning Kit (New England Biolabs). *Escherichia coli* DH5α cells were used for plasmid amplification. All restriction enzymes used in this study were purchased from New England Biolabs.

pMG6 and pMG7 were generated by excising the *GPD* or the *GAL* promotor (and the corresponding *CYC* terminator) from pRS416pGPD and pRS416pGAL (Mumberg et al., 1994, 1995), respectively, with the restriction enzymes SacI and KpnI and ligating it into pRS316 (Sikorski and Hieter, 1989) that was cut in a similar fashion.

In order to generate pMG18 and pMG88, for the expression of mCherry-CRY2, mCherry-CRY2 was amplified from pHR-mCh-Cry2olig (Shin et al., 2017) with oMG22/oMG23 and integrated into the SalI-linearized backbones of pMG6 and pMG7, respectively, via Gibson Assembly. pMG60 and pMG90 were generated by subcloning of pMG18 or pMG88 into pRS305 (Sikorski and Hieter, 1989): pMG18 or pMG88 were amplified with oMG44/oMG45, pRS305 with oMG42/oMG43 in two separate PCR reactions and the two products were fused via Gibson Assembly.

For pMG148, expressing 97Q-Opto, Huntingtin exon 1 including an N-terminal cMyc tag as well as the C-terminal poly-proline region was amplified from pYES2-myc-97QmCh (Park et al., 2013) with oMG113/oMG114 and fused with the pMG60 backbone amplified with oMG111/oMG112 via Gibson Assembly. pMG150, for the expression of 97Q-mCherry, was generated based on pMG148: pMG148 was amplified with oMG113/oMG143 as well as oMG88/oMG112 in two separate PCR reactions. The PCR products were ligated via Gibson Assembly.

pMG154 and pMG155, for the expression of 20Q-Opto or 20Q-mCherry, respectively, were generated by excising Huntingtin exon 1 including the N-terminal cMyc tag as well as the C-terminal poly-proline region from pYES2-myc-20QmCh (Park et al., 2013) with EcoRI and BglII and ligating it into the backbones generated by amplifying either pMG148 or pMG150 with oMG146/oMG147 via Gibson Assembly.

In order to generate pMG160, for the expression of 97Q-GFP from pRS304, a two-step approach was taken. First, GFP was amplified with oMG149/oMG150 from pFA6aGFP(S65T)kanMX6 (Bähler et al., 1998) and integrated into a backbone generated by amplifying pMG150 with oMG148/oMG88 to obtain pMG158. Next, 97Q-GFP including its promoter was amplified from pMG158 with oMG44/oMG45 and subcloned into a backbone generated by amplifying pRS304 (Sikorski and Hieter, 1989) with oMG42/oMG43 to generate pMG160. Both steps were done using Gibson Assembly reactions.

pMG159, for the expression of 20Q-GFP from pRS305, was generated by replacing mCherry in pMG155 with GFP: GFP was excised from pMG158 with BsgI and XhoI and ligated into the pMG155 backbone that was cleaved in a similar manner. Subsequently, in order to make pMG161 for expression of 20Q-GFP from pRS304, the *LEU* auxotrophy cassette in pMG159 was replaced with the *TRP* auxotrophy marker: the *TRP* marker was excised from pRS304 (Sikorski and Hieter, 1989) with AatII and DraIII and used to replace the *LEU* marker in pMG159 that was cleaved with the same restriction enzymes.

pMG185-pMG189, for expression of mid length polyQ-mCherry, were generated in two steps: first, pBacMam2-DiEx-LIC-C-flag_huntingtin_full-length_Q36, _Q48, _Q54, _Q60 and _Q73 (Harding et al., 2019) were cleaved with XhoI and PvuI to obtain 4.5 kb fragments containing the polyQ region of interest. These fragments were purified and digested again with BsgI and StuI. The products of this second digestion were integrated into the pMG150 vector backbone, which had been digested in a similar fashion to remove the 97Q portion in this vector. To generate pMG190-pMG194 expressing mid length polyQ-Opto, polyQ stretches were excised from pMG185-pMG189 with NdeI and SpeI and ligated into the pMG148 backbone that was treated in a similar fashion to remove the 97Q region.

In order to obtain pMG202 and pMG205 for recombinant expression of GST-Htt20Q and GST-Htt54Q, respectively, we excised the polyQ regions from pMG155 and pMG187 with NdeI and XbaI. The resulting fragments were integrated into the pGEX backbone generated by amplifying pGEX-Htt53Q (Schaffar et al., 2004) with oMG169/oMG170 via Gibson Assembly.

For pMG267 and pMG268, expressing 25QΔP-Opto and 97QΔP-Opto, respectively, toxic Huntingtin exon 1 without poly-proline and including an N-terminal FLAG-tag was amplified from pYES2-Htt25Q-GFP or pYES2-Htt97Q-GFP (Ripaud et al., 2014), with oMG151/oMG152 and integrated into a backbone generated by amplifying pMG245 with oMG111/oMG112 via Gibson Assembly. pMG210, expressing 66QΔP-Opto was generated in this process coincidentally as amplification of expanded polyQ stretches via PCR may lead to a loss of Q.

In order to generate pMG245 to conditionally express mCherry-Opto from pRS426, the mCherry-Opto fragment was excised from pMG90 with KpnI and SacI and ligated into a similarly digested pRS426 vector (Christianson et al., 1992). Having created pMG245, we generated pMG246-pMG252, conditionally expressing polyQ-Opto from pRS426, by excising polyQ-Opto fragments from pMG154, pMG190-pMG194 and pMG148 with XhoI and SpeI and ligated them into the similarly digested pMG245 backbone.

pMG269, for expression of *RNQ1-GFP* from pRS306, was generated by amplifying pESC-URARnq1GFP (Kaganovich et al., 2008) with oMG199/oMG142 and ligating the resulting fragment into a backbone generated by amplifying pRS306pADH (Mumberg et al., 1995) with oMG137/oMG138.

pMG271, for expression of *RNQ1-GFP* lacking the cMyc tag, was generated by performing two separate PCR reactions with template pESC-URA-Rnq1-GFP and the primer pairs oMG207/oMG208 and oMG209/oMG210 to generate fragments with complementary overhangs excluding the cMyc tag. Fragments were fused in a Gibson Assembly reaction.

All constructs were verified by DNA sequencing.

Yeast strains

Yeast strains used in this study are listed in the key resources table.

yMG33 is the [*PIN*$^+$] parent strain from which all yeast strains with integrated expression vectors used in this study are derived. It was generated by transforming SY197 (Klaips et al., 2014) with a cassette generated by amplifying the kanamycin resistance gene from pFA6-kanMX4 with oMG1/oMG2 to delete endogenous *PDR5*. Transformants were selected by growth of cells on plates containing 300 μg/mL G418. Clones were verified by PCR.

Other [*PIN*$^+$] strains were generated based on yMG33 by integrating plasmids containing the desired gene into an auxotrophy marker locus and selecting transformants on media lacking the respective organic compound; see strain identifiers for details on host strain and plasmid used for integration (key resources table). pRS304-based plasmids were linearized with Bsu36I, pRS305 with AflII and pRS306 with StuI prior to transformation. [*pin*$^-$] strains are derived from respective [*PIN*$^+$] strains via prion curing through three passages on YPD plates containing 3 mM GdnHCl (Cox et al., 2007; Derkatch et al., 1997; Tuite et al., 1981). The exceptions are yMG103, yMG104, yMG106, yMG120, yMG132 and yMG122, where a second integrating plasmid was transformed into an already existing [*pin*$^-$] background.

The prion status of all strains was determined by transient expression of *RNQ1-GFP* and examination of Rnq1-GFP state by microscopy.

General sample handling

In order to prevent the undesired oligomerization of the Opto constructs used in this study, all culture and sample handling steps described in the following methods were performed in the absence of blue light in a dark room with red light as only light source, unless stated otherwise. Once protein denaturing conditions were applied (e.g., through the addition of SDS-PAGE sample buffer), subsequent experimental procedures were performed under regular light conditions.

Preparation of cell extracts

Generally, 30 OD_{600} equivalents of cells were harvested at log phase growth, unless stated otherwise. Cell pellets were washed once with ice-cold water and resuspended in lysis buffer (10 mM Tris pH 7.5, 150 mM NaCl, 0.5 mM EDTA, 0.5% IGEPAL CA-630, 5% glycerol, 1 mM PMSF, Complete Protease Inhibitor Cocktail, EDTA-free). An equal volume of glass beads was added and cells

were lysed by vortexing 3 x 20 s using a FastPrep-24 bead beating grinder (MP Biomedicals). Cell lysates were cleared by centrifuging twice at 500 x g for 5 min at 4 °C. Total protein concentration of cell lysates was determined using the Pierce Rapid Gold BCA Protein Assay Kit (Thermo Scientific) or Bio-Rad Protein Assay Kit (Bio-Rad Laboratories).

Mass spectrometry

Total proteome analysis

Cell pellets were lysed in lysis buffer (100 mM Tris pH 8.0, 1% sodium deoxycholate, 40 mM 2-cloroacetamide, 10 mM tris(2-carboxyethyl)phosphine) by incubation at 95 °C for 2 min and subsequent sonication using a Bioruptor Plus sonication device (Diogenode) for 10 x 30 s at high intensity. Before digestion, the samples were diluted 1:4 with water. Samples were digested for 4 h at 37 °C with 1 μg of LysC and overnight at 37 °C with 1 μg trypsin (Promega). The peptide mixture was acidified with trifluoroacetic acid (TFA) to a final concentration of 1%, followed by desalting via home-made SCX StageTips (Rappsilber et al., 2007). Samples were vacuum dried and re-suspended in 6 μl 0.1% formic acid.

Rnq1-GFP interactome analysis

[*PIN*$^+$] or [*pin*$^-$] yeast cells carrying a plasmid encoding *RNQ1-GFP* under the control of a galactose-inducible promoter were grown in SCRaf medium overnight and back diluted the next morning. Four hours before harvesting, expression of *RNQ1-GFP* was induced by the addition of galactose to the growing cultures to a final concentration of 2%. Cells were harvested during log phase growth. Cells were lysed as described above in Triton lysis buffer (10 mM Tris pH 7.5, 150 mM NaCl, 0.5 mM EDTA, 0.2% Triton X-100, 5% glycerol, 1 mM PMSF, Complete Protease Inhibitor Cocktail, EDTA-free) instead of regular IGEPAL-containing lysis buffer, following a protocol described by Fan et al. (2004). 2 mg of total protein were mixed with 50 μL anti-GFP μMACS beads (Miltenyi Biotec) and samples were rotated at 4 °C for 1 h. Magnetic beads were separated using μMACS columns (Miltenyi Biotec). Beads were washed 3 times with Triton lysis buffer and twice with wash buffer (20 mM Tris pH 7.5). Proteins were predigested on the column by addition of elution buffer 1 (2 M urea, 50 mM Tris pH 7.5, 1 mM DTT, 5 μg/mL trypsin) and incubation at room temperature for 30 min. Proteins were eluted from the column by the addition of elution buffer 2 (2 M urea, 50 mM Tris pH 7.5, 5 mM chloroacetamide). The digestion reaction was allowed to continue overnight at room temperature and was stopped the next morning by the addition of TFA to a final concentration of 1% followed by desalting via home-made SCX StageTips (Rappsilber et al., 2007). Samples were vacuum dried and re-suspended in 6 μl 0.1% formic acid.

97Q-Opto interactome analysis

[*PIN*$^+$] or [*pin*$^-$] yeast cells expressing 97Q-Opto were grown in the respective light condition for at least 18 h. Cells were harvested during log phase growth and lysed as described above. Samples were split into a total and a soluble sample by centrifugation at 15'000 x g for 15 min at 4 °C. 4 mg of total protein were mixed with 50 μL anti-c-Myc μMACS beads (Miltenyi Biotec) and samples were rotated at 4 °C for 1 h. Beads were washed 3 times with lysis buffer and twice with wash buffer (20 mM Tris pH 7.5). The on-column trypsin digest and subsequent sample preparation steps were performed as described above for Rnq1-GFP.

LC-MS/MS

Peptides were loaded onto a 30 cm column (inner diameter: 75 microns; packed in-house with ReproSil-Pur C18-AQ 1.9 micron beads, Dr. Maisch GmbH) via the autosampler of the Thermo Easy-nLC 1200 (Thermo Scientific) at 60 °C. Eluting peptides were directly sprayed onto the benchtop Orbitrap mass spectrometer Q Exactive HF (Thermo Scientific). Liquid chromatography with the Easy-nLC 1200 was performed by loading the peptides in buffer A (0.1% formic acid) at a flow rate of 1.25 μl min^{-1} and peptides were separated with a flow rate of 250 nL min^{-1} by a gradient of buffer B (80% ACN, 0.1% formic acid). For the total proteome analysis, a gradient from 2% to 30% over 120 min was used, followed by a ramp to 60% over 10 min, then 95% over the next 5 min and finally, the percentage of buffer B was maintained at 95% for another 5 min. For the interactome analyses, different parameters were used: here, a gradient from 7% to 30% over 60 min was followed by a ramp to 60% over 15 min, then 95% over the next 5 min and finally the percentage of buffer B was maintained at 95% for another 5 min.

The mass spectrometer was operated in a data-dependent mode with survey scans from 300 to 1750 m/z (resolution of 60'000 at m/z =200), and up to 15 (for total proteome)/10 (for interactomes) of the top precursors were selected and fragmented using higher energy collisional dissociation (HCD with a normalized collision energy value of 28). The MS2 spectra were recorded at a resolution of 15'000 (at m/z = 200). AGC target for MS1 and MS2 scans were set to 3 x 10^6 and 1 x 10^5, respectively, within a maximum injection time of 100 and 25 ms (for total proteome)/60 ms (for interactomes) for MS1 and MS2 scans, respectively.

Data analysis

Raw data were processed using the MaxQuant computational platform with standard settings applied. Briefly, the peak list was searched against the Uniprot database of *Saccharomyces cerevisiae* with an allowed precursor mass deviation of 4.5 ppm and an allowed fragment mass deviation of 20 ppm. MaxQuant by default enables individual peptide mass tolerances, which was used in the search. Cysteine carbamidomethylation was set as static modification, and methionine oxidation and N-terminal acetylation as variable modifications. The match-between-run option was enabled, and proteins were quantified across samples using the label-free quantification algorithm in MaxQuant generating label-free quantification (LFQ) intensities. Analysis and visualization of mass spectrometry results was performed using the Perseus software platform and GO Enrichment Analysis.

Cycloheximide chase

Cells were grown for 18 h with occasional back dilution. For *SIS1* shut-off, doxycycline was added to the medium to a final concentration of 10 μg/mL. Once cells reached log phase growth, 25 OD_{600} equivalents of cells were pelleted and resuspended in media containing 0.5 mg/mL cycloheximide. Cells were further incubated at similar growth conditions as before. At indicated time points, 4.5 OD_{600} equivalents of cells were removed, pelleted and flash frozen for further analysis.

Alkaline lysis and TCA precipitation

Cell pellets were resuspended in 1 mL ice cold water. 150 μL alkaline lysis buffer (138.75 μL 2 M NaOH + 11.25 μL β-Mercaptoethanol) were added and cell suspension was incubated on ice for 5 min, with occasional vortexing. Samples were further incubated on ice for 15 min after addition of 10 μL sodium deoxycholate (at 2% w/v). 100 μL 100% trichloroacetic acid were added, reactions were vortexed and incubated on ice for 30 min. Samples were pelleted by centrifugation at 20'000 x g for 30 min at 4 °C. Pellets were washed with ice cold acetone and air dried. 100 μL HU buffer (8 M urea, 200 mM Tris pH 6.8, 1 mM EDTA, 5% SDS, 0.03% bromphenol blue, 100 mM DTT) were added and samples shaken for 15 min at 1'400 rpm and 70 °C to resolubilize the pellets, followed by analysis by SDS-PAGE.

SDS-PAGE

Protein samples were mixed with an equal volume of 2x SDS-PAGE sample buffer (100 mM Tris pH 6.8, 4% SDS, 20% glycerol, 0.03% bromophenol blue, 200 mM DTT) and heated for 5 min at 95 °C. Samples were analyzed using NuPAGE 4-12% Bis-Tris gels and NuPAGE MOPS SDS running buffer (both Invitrogen). Gels were run at 200 V for 55 min.

SDD-AGE

Yeast cell lysates were prepared as described above (see preparation of cell extracts). Samples were mixed with 4x SDD-AGE sample buffer (240 mM Tris pH 6.8, 8% SDS, 15% glycerol, 0.03% bromophenol blue) and incubated at 30 °C for 7 min. Proteins were resolved on an agarose gel (1.5% agarose, 20 mM Tris base, 200 mM glycine, 0.1% SDS) using SDD-AGE running buffer (20 mM Tris base, 200 mM glycine, 0.1% SDS) at 125 V for 105 min at 4°C.

Immunoblotting

Protein gels were electroblotted on Amersham Protran Western blotting membranes (Merck) in SDS-PAGE transfer buffer (25 mM Tris, 192 mM glycine, 20% methanol, 0.037% SDS) for 2 h at 70 V for SDS-PAGE or in SDD-AGE transfer buffer (25 mM Tris, 192 mM glycine, 20% methanol, 0.01% SDS) for 14.5 h at 7 V for SDD-AGE gels. Membranes were washed with TBS-T (10 mM Tris pH 7.4, 150 mM NaCl, 0.1% Tween20), blocked in 5% milk in TBS-T (w/v) and incubated with primary antibodies in 5% milk in TBST (w/v) at 4 °C overnight. Membranes were washed with TBS-T and incubated with secondary HRP antibodies in TBS-T at room temperature for 1 h. After a final wash with TBS-T, chemiluminescence of secondary antibodies was visualized with Immobilon Classico Western HRP substrate (Millipore) using an Amersham ImageQuant 800 Western blot imaging system (Cytiva Life Sciences). Image processing and densitometric analyses were carried out using the Fiji-ImageJ Image processing package. For stripping of antibodies, membranes were incubated in Restore Western Blot Stripping Buffer (Thermo Scientific) for 10 min at 60 °C, followed by incubation for 20 min at room temperature. Membranes were washed thoroughly with TBST and immunoblotted as described above.

β-Galactosidase activity assay

β-Galactosidase activity assays were performed according to Rupp (2002). To analyze the induction of the cytosolic HSR, respective yeast cultures carrying an additional plasmid encoding β-galactosidase under the control of a promotor with integrated heat shock elements were grown in SC medium in various conditions further specified in the respective figure legends. For experiments related to Figures 1F, S2B, and S4C, cultures were shifted to the indicated temperatures for one hour prior to harvest. Once cells reached log phase growth, 3 OD_{600} equivalents of cells were harvested and lysed by incubation in Z-buffer (100 mM NaH_2PO_4/Na_2HPO_4 pH 7.0, 10 mM KCl, 1 mM $MgSO_4$, 2 mM β-mercaptoethanol, 0.01% SDS, 6.25% chloroform) at 30 °C for 5 min. β-Galactosidase substrate 2-nitrophenyl β-D-galactopyranoside (ONPG) was added to a final concentration of 0.8 mg/mL and reactions incubated for 5-8 min at 30 °C before stopping by addition of $NaCO_3$ to a final concentration of 300 mM. Absorbance at A_{420} was measured on a photometer and β-galactosidase activity, expressed in Miller units (MU), was calculated as: 1000*((A_{420})/(OD_{600} harvested * ONPG incubation time)).

Confocal imaging

Cells from log phase cultures were fixed by addition of formaldehyde to a final concentration of 3% for 5 min. Fixed cells were applied to the chamber of a concanavalin A-coated μ-Slide (Ibidi) and allowed to adhere for 5 min at room temperature. After washing with PBS to remove non-adherent cells, cells were imaged on an Olympus FV1000 confocal microscope (Olympus) equipped with a Zeiss Plan-Apochromat 63x/1.4 Oil DIC M27 objective (Carl Zeiss). For detection of the GFP fluorophore an excitation wavelength of 488 nm and emission of 505-540 nm was chosen. For the mCherry fluorophore, wavelengths of 559 nm for excitation and 575-675 nm for emission were used. Image analysis was carried out using the Fiji-ImageJ Image processing package.

To analyze the reversibility of light induced protein clusters, log phase yeast cultures expressing polyQ-Opto proteins were illuminated with blue light for 5 min and returned to the dark for further incubation. At indicated time points, cells were fixed and applied to the chamber of a μ-Slide as described above. Using the EPI fluorescence light on the microscopic setup (see above), the number of cells with visible inclusions was counted manually. 100 cells were counted for each single replicate data point.

Filter retardation assay

Filter retardation assays were performed essentially as described (Scherzinger et al., 1997; Muchowski et al., 2000). Yeast cell lysates were prepared as described above (see preparation of cell extracts). Samples were diluted to the same protein concentration in lysis buffer and incubated with 100 U DNase for 30 min at 4 °C. When indicated, SDS/DTT was added to a final concentration of 2%/50 mM and the samples were heated at 95 °C for 5 min. Control samples were only diluted with equal volumes of lysis buffer and were not boiled. Samples treated with formic acid were first precipitated with 25% trichloroacetic acid (TCA) before resuspension in 100% formic acid at 37 °C for 30 min (Hazeki et al., 2000). Formic acid was evaporated and samples resuspended in SDS/DTT and boiled as described above. Samples were applied to a 0.2 μm pore size cellulose acetate membrane (Cytivia Life Sciences), pre-wetted in 0.1% SDS, in a PR648 Slot Blot Blotting Manifold (Hoefer) and washed 3 times with 0.1% SDS. Retained material on the membrane was visualized by immunoblotting. Densitometric analyses were carried out using the Fiji-ImageJ Image processing package.

Cell fractionation

Yeast cell lysates were prepared as described above (preparation of cell extracts). Soluble fractions were prepared by centrifugation at 15'000 x g for 15 min at 4 °C. Total and soluble lysate fractions were analyzed via SDD-AGE, SDS-PAGE and filter retardation analysis.

Growth assay

Yeast cells expressing toxic polyQΔP-Opto constructs were cultured in inducing media for 40 h with frequent back-dilution to ensure stable expression levels. OD_{600} values were then measured at regular time points during logarithmic growth. Growth curves were fit with exponential equations in GraphPad Prism to obtain doubling times.

FACS analysis

To determine the expression levels of toxic polyQΔP-Opto constructs, yeast cells were cultured in inducing media for 48 h with frequent back-dilution to ensure stable expression levels. Once cells reached log phase growth, 5 OD_{600} equivalents of cells were harvested, washed twice with PBS (175 mM NaCl, 8.41 mM Na_2HPO_4, 1.86 mM NaH_2PO_4) and resuspended in PBS. Cells were analyzed with an Attune NxT Flow Cytometer (Thermo Scientific) using the 561 nm laser for detection of the mCherry fluorophore. Average fluorescence value was used as a measure for expression level.

Recombinant protein expression

Expression plasmids for GST-Htt20Q (pMG202) or GST-Htt54Q (pMG205) were transformed into competent *Escherichia coli* Dl21 (DE3) cells for recombinant expression. Bacteria carrying the expression plasmids were grown in terrific broth media (12 g tryptone, 24 g yeast extract, 5 mL glycerol, 72 mM K_2HPO_4, 17 mM KH_2PO_4) at 37 °C. Once cultures reached an OD_{600} of ~0.4, flasks were transferred to 18 °C. Isopropyl β-D-1-thiogalactopyranoside (IPTG) was added to a final concentration of 0.4 mM to induce expression and cultures were further incubated overnight. Cells were harvested and washed once with ice cold PBS.

Recombinant protein purification

Recombinant protein purification of GST-Htt20Q and GST-Htt54Q was performed as described (Muchowski et al., 2000; Scherzinger et al., 1997). All protein purification steps were performed on ice or at 4 °C. Cell pellets were resuspended in buffer A (50 mM NaH_2PO_4 pH 7.4, 150 mM NaCl, 1 mM EDTA, Complete Protease Inhibitor Cocktail, EDTA-free). Lysozyme was added to a final concentration of 1 mg/mL, DNase to a final concentration of 2.5 U/mL and the cell suspension was incubated for 45 min. Cells were lysed through multiple passages on an EmulsiFlex-C5 high pressure homogenizer (Avestin). n-Octyl-β-D-glucopyranoside (OGP) was added to a final concentration of 0.1%, followed by incubation for 5 min. Cell debris was pelleted by centrifugation at 125'000 x g for 1 h at 4 °C using a Type 45 Ti Fixed-Angle Titanium Rotor (Beckman Coulter). Supernatant was applied onto a GSTPrep Fast Flow 16/10 (Cytiva Life Sciences) affinity column that was pre-equilibrated in buffer B (50 mM NaH_2PO_4 pH 7.4, 150 mM NaCl, 1 mM EDTA, 1% OGP)). The column was washed with 5 column volumes (CV) of buffer B before eluting the protein with 2 CV of buffer C (50 mM NaH_2PO_4 pH 7.4, 150 mM NaCl, 1 mM EDTA, 15 mM glutathione). Fractions containing the GST-polyQ protein were pooled and concentrated using a Vivaspin 6 30 kDa concentrator (Cytiva Life Sciences). The concentrated protein sample was applied onto a HiPrep 26/60 Sephacryl S-100 HR (Cytiva Life Sciences) size exclusion column pre-equilibrated in SEC buffer (50 mM Tris pH 7.4, 150 mM NaCl, 1 mM EDTA, 5% glycerol, 1 mM DTT). Fractions containing GST-polyQ were pooled, the quality of the purification assessed via SDS-PAGE, and the concentration of the purified protein determined with a NanoDrop One/OneC microvolume UV-vis spectrophotometer (Thermo Scientific). Glycerol was added to a final concentration of 10%. Aliquoted protein samples were snap frozen in liquid nitrogen and stored at -80 °C.

In vitro aggregation assay

For *in vitro* aggregation reactions, purified GST-polyQ was diluted to a final concentration of 3 μM with *in vitro* reaction buffer (10 mM Tris pH 7.5, 150 mM NaCl, 0.5 mM EDTA, 1 mM DTT, 1 mM PMSF, Complete Protease Inhibitor Cocktail, EDTA-free) in a total reaction volume of 1 mL. To start the reaction, GST-PreScission protease (25 U) was added, followed by inverting the tube 10 times. Samples were then incubated at 30 °C and shaking at 300 rpm. At indicated time points samples were taken for analysis by SDD-AGE, SDS-PAGE or filter retardation assay. For analysis by SDD-AGE, 75 μL of sample were mixed with 4x SDD-AGE sample buffer (240 mM Tris pH 6.8, 8% SDS, 15% glycerol, 0.03% bromophenol blue). SDS-PAGE samples were generated by adding 20 μL of aggregation reaction to an equal volume of 2x SDS-PAGE sample buffer (100 mM Tris pH 6.8, 4% SDS, 20% glycerol, 0.03% bromophenol blue, 200 mM DTT) and heating at 95 °C for 5 min. For analysis by filter retardation assay, 200 μL of the reaction were mixed with an equal volume of 4% SDS/100 mM DTT and heated at 95 °C for 5 min. All samples were flash frozen in liquid nitrogen and stored at -80 °C until further analysis.

For *in vitro* aggregation assays in the presence of cell lysate, yeast strains with and without overexpression of *RNQ1-GFP* were harvested at log phase growth. Cells were lysed as described above (see preparation of cell extracts) but *in vitro* reaction buffer (see above) was employed instead of the detergent-containing lysis buffer used otherwise in this study. For the aggregation assays, GST-Htt54Q protein was diluted into cell lysate. The final lysate protein concentration was 4.4 mg/mL. Aggregation assays were otherwise performed as described above.

Aggregation assays described in Figures 6F, 6G, and S6F were performed in the presence of anti-GFP immunoprecipitation beads preloaded with Rnq1-GFP. GFP-Trap agarose beads (400 μL; ChromoTek) were incubated overnight at 4 °C with 4.4 mg total lysate from [*pin*$^-$] or [*PIN*$^+$] cells overexpressing *RNQ1-GFP* in a total reaction volume of 1.4 mL. Beads were separated at 2'500 x g for 5 min at 4 °C and washed twice with *in vitro* reaction buffer. For the aggregation reaction, GST-Htt54Q protein was diluted into [*pin*$^-$] cell lysate in a total volume of 1 mL as described above and mixed with 400 μL Rnq1-GFP-loaded beads. The aggregation reaction was started by the addition of GST-PreScission protease (25 U), followed by incubation with end-over-end rotation at 10 rpm and 30 °C. At indicated time points, beads were sedimented at 500 x g for 5 min and samples for SDD-AGE taken from the supernatant fraction. Samples were treated and analyzed as described above.

QUANTIFICATION AND STATISTICAL ANALYSIS

LC-MS/MS experiments were performed in quadruplicates. For the total proteome analysis in Figure 1B, *p*-values for volcano blots were calculated by Student's *t*-test for proteins detected in all four biological replicates in each group. For the interactome analyses in Figures 1C, 1D, 5, and S5, proteins detected in three biological replicates in at least one group were considered. Enrichment of > 1.5-fold with p-value < 0.05 was indicated as significant.

For all other quantitative experiments where statistical analyses were performed, details can be found as annotations in the figures (p-values) and the corresponding figure legends (number and definition of n as well as center and dispersion of data). Statistical analysis and representation of quantitative data was performed using GraphPad Prism. For all statistical analyses, two-way ANOVA was used with Bonferroni's multiple comparisons test. p-values < 0.05 were considered significant.

Densitometric quantifications were performed using the Fiji-ImageJ Image processing package.